Performance Analysis and Optimal Resource Allocation for Large Scale Joint Sensing and Communication

Jiajie Xu[1], *Member, IEEE,* Mustafa A. Kishk[2], *Member, IEEE,* Justin P. Coon[3], *Senior Member, IEEE,* Mohamed-Slim Alouini[1], *Fellow, IEEE*

***Abstract*—Joint sensing and communication (JSAC) is regarded as a promising technology for future networks, which can reuse most devices of the systems in sensing and communication (S&C) and reduces the cost in terms of power and spectrum (P&S) critically. The current research considers the P&S allocation of S&C separately and then discusses the performance from different aspects. However, as an integrated system, the allocation strategy of P&S allocation affects the joint performance significantly. In this article, we use tools from stochastic geometry to study the coverage performance considering the trade-off of P&S allocation for JSAC with the principle requirements of small distance resolution (SDR) in sensing and high data rate (HDR) in communication. In particular, we model the locations of user equipment (UE) and base stations (BSs) as two different Poisson Point Processes and allocate P&S at BSs with two independent ratios. The sensing system will detect the surrounding environment and obtain UE positions. After that, an adaptive beamwidth for beamforming technology is applied in communication, which can save energy effectively. First, we introduce the distance resolution in sensing and special channel models in S&C with a high frequency. Then, considering the proposed system model, we separately model the interference in S&C. Further, the joint coverage probability (CP) of JSAC is derived as a function of densities of UE and BSs, required HDR and SDR, and allocation ratios of P&S. Finally, We draw multiple valuable system-level insights from the proposed analysis. For instance, we show that the SDR and HDR are the two main constraints to the maximum achievable CP with optimized allocations of P&S. Furthermore, we show that different densities of BSs should be considered in various scenarios. The revealed relationship between the densities of UE and BSs can be taken as a reference in practical applications.**

***Index Terms*—Joint sensing and communication, Stochastic geometry, Coverage probability, Trade-off, Power allocation, Spectrum allocation, Adaptive beamwidth.**

I. Introduction

A. Motivation

Current communications and localization systems, such as the fifth-generation (5G) communication network and the target detection/localization/navigation system with radar or lidar, tend to be independent. With the development of communication using high frequency (mmWave or THz) [1], [2], the spectrum overlaps between communication and detection. Considering the units involved in the two systems, like amplification, filter, etc., communication and detection share the same devices and similar technologies at a certain level. Besides that, if information on detection and communication systems can be mutually used, extra gains can be achieved [3], [4]. Naturally, combining sensing (detection/localization) and communication (S&C) into one system to reduce the cost of the device was proposed, which is named joint sensing and communication (JSAC) or integrated sensing and communication (ISAC). In the past few years, JSAC has attracted a lot of attention in the next-generation network from both academia and industry [5]–[9]. Thinking from another angle, the high-frequency S&C leads to a small coverage range, which means a high density of base stations (BSs) is required. Given that the application scenarios that use S&C relatively cover large areas, the amount of BSs required is significant. In this way, the adhibition of JSAC can lead to substantial cost savings, including the cost of the hardware device, energy, and spectrum [4], [10], [11].

Since cost-saving is pivotal in JSAC, the allocation of P&S and the density of nodes, including densities of user equipment (UE) and BSs, need to be paid extra attention. In the existing literature, some of the works focus on the performance of JSAC, such as throughput, and beamforming design, to name a few [12]–[17]. However, few works focus on the coverage performance of JSAC in a practical application scenario, especially from a statistical point of view, to analyze the coverage performance considering the joint properties in terms of P&S. To the best of our knowledge, this is the first work to analyze the coverage performance of JSAC considering the allocations of P&S, reveal the effects made by the various densities of UE and BSs, and explore the gain achieved by S&C. More details about the contributions of this article will be presented in Sec. I-C. First, we enlist the related work in the next subsection.

B. Related work

In this subsection, we discuss the most related works in literature, which can be categorized into: (i) stochastic geometry-based design and analysis of JSAC, (ii) performance trade-off in JSAC.

Stochastic geometry-based design and analysis of JSAC. The fluctuation of the target radar cross-section (RCS) is

[1] Computer, Electrical, and Mathematical Science and Engineering Division, King Abdullah University of Science and Technology, Thuwal, Saudi Arabia, [2] Department of Electronic Engineering, Maynooth University, Maynooth, Ireland, [3] Department of Engineering Science, University of Oxford, Oxford, U.K., (e-mail: jiajie.xu.1@kaust.edu.sa, mustafa.kishk@mu.ie, justin.coon@eng.ox.ac.uk, slim.alouini@kaust.edu.sa).

modeled in [18], where mmWave radar is applied to detect the vehicles on a practical bi-directional multi-lane road. Vehicle-to-vehicle interference and the beamwidth of the radar signal are considered. The analysis results reveal that the characteristics of radar affect the target ranging performance a lot. A mathematical framework is proposed in [19] to characterize the JSAC coverage probability (CP) and ergodic capacity. BSs, UE, and sensing targets (STs) are involved in the proposed framework. An information-theoretic formulation of radar tracking is employed, and a shared multicarrier waveform and analog beamforming are used to analyze the downlink S&C coverage and capacity. In [20], BSs, UE, radars, and targets are involved in constructing JSAC. A bistatic target-sensing process is characterized where a straight signal transmitted by BS is received by the radar, and an echo signal (which is transmitted by the BS) reflected by the target is received by the radar. Fusion analysis of the straight and the echo signals is achieved at the side of the radar in order to localize the target. Authors in [21] analyze the average cooperative detection range in the application scenarios of JSAC. Different numbers of vehicles with sensing and communication devices are placed randomly. The sensing range and communication range are given. Hence, the average overlaps of the sensing and communication regions can be calculated in different scenarios, such as two vehicles, three vehicles, and more. Authors in [22] consider an automotive scenario including a two-lane road with vehicles and smart traffic lights. All the vehicles and traffic lights are equipped with a dual-function radar and communication system. Multiple metrics are considered to evaluate the performance of JSAC, such as communication CP, radar false alarm probability, radar detection probability, radar success probability, joint radar detection and communication CP, and joint radar success and communication CP. In [23], multi-radar cooperative detection is proposed to expand the detection region. At the same time, communication links between radars are established. In the application scenario, all the radars are divided into different tiers. In each tier, one of the radars will be selected as the fusion center. Other radars in the same tier will detect the target, collect the information about the target, and then transmit the gathered information to the fusion center. Power allocation for radar detection and communication is considered. The cooperative detection region of the multi-radar is analyzed since there will be some overlap detection regions for different radars. From [19] to [23], authors notice the necessity of stochastic geometry to model the randomness of nodes, including UE, BSs, and targets, and design different models for various application scenarios, and then analyze the proposed JSAC. However, in all the discussed literature, the characteristics of "Joint/Integrated" are not presented, and the trade-off between sensing and communication is not considered, which is one of the most critical characteristics of JSAC. Authors in [24] divide the network area into hexagonal cells, and a joint radar and communication node is placed at the cell centers. Stochastic geometry is applied to describe the nodes' location, including base stations and mobile users. Communication coverage and radar detection probabilities, as well as the throughput, are analyzed.

Performance trade-off in JSAC. Authors in [25] apply pulse radars in a network for target detection and data exchange. The two functions share the same wireless channel. Based on stochastic geometry tools, radar detection range and network throughput are studied. Particularly, the time-division method is applied. Pulse radars share a common bandwidth, and each of them operates in turn in radar mode (detect targets) and in communication mode (data exchange). The timeline is slotted, and pulse radars access the shared channel following a slotted ALOHA policy. In [26], effects over the network throughput made by time trade-off are analyzed in JSAC. Parameters involved in radar sensing using pulse signals, such as the exploitation duty cycle, the radar bandwidth, the transmit power, and the pulse repetition interval, are considered. A bistatic sensing model is considered in [26], where the BS transmits the sensing or communication signal with a time division schedule. The mobile user (sensing target) will reflect the sensing signal to the receiver, which is also the receiver of communication. Authors in [27], [28] analyze the trade-off of power between S&C and propose a unified passive radar and communication system. Constrained by the total power, the probability of detection is maximized while satisfying the information rate required by the communication receiver. Although, in the mentioned literature, the performance trade-off in JSAC is discussed at a certain level, the gains of JSAC are not explored to the end. Besides the trade-off, the gain obtained by S&C from joint operation should be considered.

C. Contributions

In this article, we use tools from stochastic geometry to analyze the coverage performance of JSAC, considering the trade-off of power and spectrum (P&S), achieving extra gains of S&C from joint operation while satisfying the requirements of small distance resolution (SDR) in sensing and high data rate (HDR) in communication. We study the ergodic optimized allocation of P&S and effects made by various densities of UE and BSs. The contributions are presented as follows.

- We propose a framework that takes joint consideration of the P&S into coverage performance analysis in JSAC while considering the requirements of distance resolution in sensing and data rate in communication.
- We investigate the potential gains obtained from information sharing among sensing and communication systems. With the assistance of sensing, beamforming technology can be applied in communication, and an adaptive beamwidth strategy is designed to improve the energy efficiency of communication based on the location information provided by the sensing system.
- Assisted by the derived performance metrics and the numerical results, we draw various system-level insights. For instance, considering a given density of the UE, with the ergodic optimized allocation of P&S, the density of BSs can be optimized to achieve the best CP. When we do not have enough resources, including P&S, suggestions are provided on which SDR or HDR should be sacrificed first.

The remainder of this article is organized as follows. In Sec. II, we give a brief background on JSAC, including the distance resolution in the target sensing and the channel models for S&C separately. In Sec. III, the structure of the joint system, as well as the interference in S&C scenarios, and the allocation of energy and spectrum, are discussed in detail. In Sec. IV, the CPs of sensing, communication, and JSAC are calculated. Numerical results generated by Monte-Carlo simulations are illustrated in Sec. V to corroborate the proposed analysis and insights. Finally, Sec. VI concludes this article and discusses some future work.

The Notations used in this paper are explained in Table I.

TABLE I: Table of Notations and Descriptions.

Notation	Description
P_t, B	The total transmit power and bandwidth
$\gamma_{bs}, \gamma_{st}, \gamma_{sct}$	Densities of BS, ST, and SCT
$d'_{s,res}$	Maximum distance resolution in sensing
$g_{s,t}, g_{s,r}$	Antenna gains at transmitter and receiver
$\rho_{st}, \rho_{st,i}$	Radar cross section
T_c	Duration time of the chirp signal
N	The number of chirps
F_n	Noise figure at the receive antenna in sensing
$r'_{c,com}$	Minimum data rate in communication
$L_{gas} + L_{rain}$	Path loss for gas and rain
L_{add}, L_{imp}	Additional loss and implementation loss
C_d	The cover diameter in communication
N_0	Noise power spectral density
g_{cb}	Beamforming gain in communication

II. Background

In JSAC, radar detection and high-frequency communication are applied. In this article, we take the bandwidth of 77 GHz to 81 GHz into the analysis process. Considering the different characteristics of millimeter waves, a background of the distance resolution of radar detection and channel models for S&C are introduced.

A. Distance resolution in target sensing

In JSAC, to achieve SDR, a normal Frequency-Modulated Continuous-Wave (FMCW, which is also named a chirp signal) is transmitted by a BS, which can be shown in Fig. 1 as the blue line. The start frequency is f_0, the bandwidth is B_s, the chirp time is T_c, so the slope of the spectrum is $S = \frac{B_s}{T_c}$. When the chirp signal from the transmitter touches some targets, the signal will be reflected back to the transmitter, the BS, for example, the red line (Target 1), the green line (Target 2), and the manganese line (Target i). t_1, t_2, and t_i mean the different time delays created by the distance between the BS and different targets. Based on Fig. 1, we know that multiple

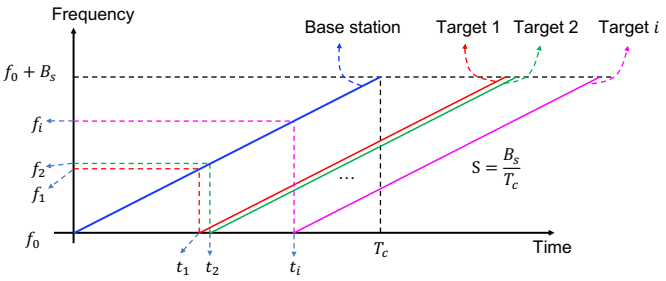

Fig. 1: A normal Frequency-Modulated Continuous-Wave.

targets can be sensed by BS easily, and the distance resolution can be derived as follows.

For the transmitted signal, we can model it as:

$$x_{\mathrm{BS}} = \sin\left(2\pi(f_0 + St)t + \phi_0\right), \quad 0 \le t \le T_c. \tag{1}$$

For the echo signal from target 1, we can model it as:

$$x_{\mathrm{T}_1} = \sin\left(2\pi(f_1 + St)t + \phi_1\right), \quad t_1 \le t \le t_1 + T_c. \tag{2}$$

At the same time as BS transmits the sensing signal, the transmitted signal will be sent to the mixer. When the BS receives the echo signal from target 1, the received signal will also be sent to the mixer, and then we can get the intermediate frequency (IF) signal as follows:

$$x_{\mathrm{IF}} = \sin\left(2\pi(|f_0 - f_1|)t + (\phi_0 - \phi_1)\right), \quad t_1 \le t \le T_c. \tag{3}$$

Hence, the frequency of the IF signal, $|f_0 - f_1| = S \times t_1$, is a constant that is directly proportional to the time delay (i.e., the distance between BS and target 1). Hence, the distance between the BS and the target can be calculated as follows:

$$d_1 = 0.5ct_1, \tag{4}$$

where $c = 3 \times 10^8$ m/s. Normally, in the detection system, the receiver antenna is an array. Hence, multiple distances (from each antenna in the array) to the target can be achieved, and then the target's location can be calculated.

Regarding the multi-target scenario, distance resolution must be considered, which means the minimum distance difference between two targets that makes the distinction between the two targets possible. We can assume that target 2 is slightly further away from BS than target 1. In reference to the IF signal frequency in (3), the difference in frequency between the IF signals of target 1 and target 2 is $|f_1 - f_2|$. Let $\Delta f = |f_1 - f_2|$ and we can have

$$\Delta f = S \times \Delta t = S \times \frac{2\Delta d}{c}, \tag{5}$$

where S is the slope of the spectrum, Δd is the distance between target 1 and target 2. Since the time difference includes forward and backward times, $2\Delta d$ is considered. Recall the theory of Fourier transforms. There will be a minimum observation time if we want to distinguish two sinusoidal signals with different frequencies. Hence, we have

$$\frac{S2\Delta d}{c} > \frac{1}{T_c - t_1}$$
$$\Rightarrow \Delta d > \frac{c}{2S(T_c - t_1)} = \frac{cT_c}{2B_s(T_c - t_1)} = \frac{cT_c}{2B_s(T_c - \frac{2d_1}{c})},$$

where d_1 is the distance between BS and target 1. Hence, we can have the distance resolution in sensing at a distance d

away from the BS as:

$$d_{s,res}(d) = \frac{cT_c}{2B_s(T_c - \frac{2d}{c})}. \quad (6)$$

Considering the link in JSAC, the BS can transmit sensing and communication signals to the targets around it. In terms of sensing, BS can broadcast the sensing signal (FMCW signal) and receive the echo from the targets, and then it can obtain the locations of surrounding targets, which are noted as sensing targets. It should be marked that with the increase of the sensing distance, the distance resolution, $d_{s,res}$, increases. The coverage performance of sensing and distance resolution is related to the allocated bandwidth.

B. Channel model for target sensing

A radar is used for target sensing, and as shown in [29], the received power at the target can be written as

$$\tilde{P}_{s,r}(D) = \frac{P_{s,t}g_{s,t}}{4\pi D^2} \times \frac{\rho}{4\pi D^2} \times A_e, \quad (7)$$

where $P_{s,t}$ is the transmit power for target sensing, $g_{s,t} = 10^{0.1G_{s,t}}$, $G_{s,t}$ is the gain of the transmit antenna with the unit of dB, ρ is the radar cross-section (RCS), D is the sensing distance between the radar and the target, A_e is the effective area of the receiving antenna that collects a portion of the echo power returned to the radar. According to the antenna theory [29], there is a relation between the gain $g_{s,r}$ of the receiving antenna and its effective area A_e, which is $g_{s,r} = \frac{4\pi A_e}{\lambda^2}$, where $g_{s,r} = 10^{0.1G_{s,r}}$, $G_{s,r}$ is the gain of the receive antenna with the unit of dB, λ is the wavelength of the sensing signal. Hence, based on the characteristics of FMCW, we can have the sensing model as

$$P_{s,r}(D) = \frac{P_{s,t}g_{s,t}}{4\pi D^2}\frac{\rho}{4\pi D^2}\frac{g_{s,r}\lambda^2}{4\pi}NT_cH_s, \quad (8)$$

where N is the amount of the chirp in a frame of the sensing signal, T_c is the duration time of the chirp signal (as shown in Fig. 1), H_s is the channel fading, which is subject to an exponential distribution.

The thermal noise power at the receiver antenna can be written as [29] $n_s = KT_0B_sF_n$, where $K = 1.380649\times10^{-23}$ $\text{m}^2\cdot\text{kg}\cdot\text{s}^{-2}\cdot\text{K}^{-1}$ is the Boltzmann's constant, T_0 is the standard temperature of 290 K, B_s is the bandwidth for sensing, and F_n is the noise figure of the receiver antenna.

C. Channel model for communication

Since high frequency is used for communication in JSAC, the communication range will be very short compared with other normal radio-frequency communications. Hence, the normal free space wireless communication channel model is inapplicable. Another channel model that can be used for short-range outdoor radiocommunication system is proposed by the International Telecommunication Union (ITU). Recommended by [30]–[32], the path loss for the millimeter-wave propagation at frequencies above 10 GHz in the outdoor short-range field (<1 km) can be written as:

$$L_{LoS} = 20\log f - 28 + 19\log R + L_{gas} + L_{rain} \text{ dB}, \quad (9)$$

where f is in MHz, R is the propagation distance, L_{gas} and L_{rain} are attenuation by gases and by rain. According to [31], [32], L_{gas} and L_{rain} are independent of the propagation distance and only related to the signal frequency. Hence, for simplicity, without any influence on the analysis results, we can set L_{gas} and L_{rain} as the atmospheric absorption with a given value which is widely used [33]–[35]. In this paper, we assume $L_{gas} + L_{rain} = 2$ dB. Besides that, in mmWave communication with a frequency of around 70 GHz, additional loss and implementation loss should be considered [36], which will be indicated as L_{add} and L_{imp} in dB. For simplification, L_s is denoted as the summation of L_{gas}, L_{rain}, L_{add}, and L_{imp}. Hence, we can have the channel model for the communication in JSAC as

$$P_{c,r}(R) = \frac{P_{c,t} \times 10^{2.8}H_cg_{c,b}}{f^2R^{1.9} \times 10^{0.1L_s}}, \quad (10)$$

where $P_{c,t}$ is the transmit power in communication, H_c is the channel fading gain, which is subject to an exponential distribution, and $g_{c,b}$ is the gain of beamforming.

III. System Model

A. Structure of the joint system

The considered application scenario for JSAC is shown in Fig. 2. It should be in the center of a city or an area where many BSs can be placed, and a lot of UE can be served. To achieve a more intuitive mathematical analysis, the application scenario can be modeled as shown in Fig. 3, and the UE is categorized into: sensing targets (STs) and sensing-and-communication targets (SCTs). The JSAC is achieved by BSs, which can detect the surrounding environment and collect location information from targets, including STs and SCTs, and transmit data to SCTs. In Fig. 3, D_s is the sensing range of the BS, and R_c is the communication range between the SCT and the BS. Another pair of parameters considered in JSAC is the distance resolution in sensing and the data rate in communication, which are indicated as $D_{s,res}$ and $R_{c,com}$. In this paper, we propose to analyze the joint CP considering a restriction of a given maximum distance resolution $d'_{s,res}$ in sensing and a given minimum data rate $r'_{c,com}$ in communication.

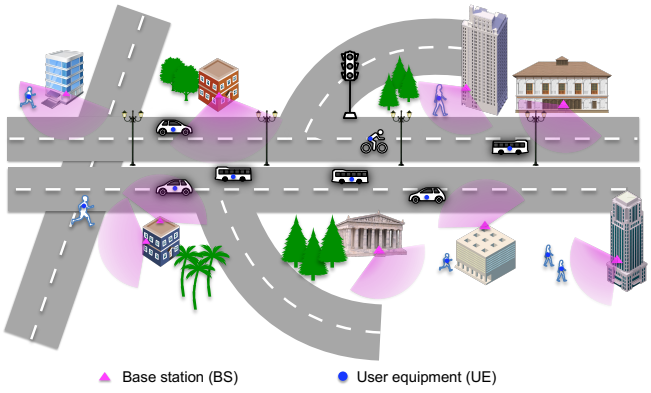

Fig. 2: Application scenario of JSAC.

Hence, we can have the joint CP with the given requirements of SDR and HDR as follows.

$$\mathbb{P}_{\text{j,cov}} = \mathbb{P}\left[\texttt{SCNR}_s \geq \tau_s, D_{s,res} \leq d'_{s,res}, \texttt{SINR}_c \geq \tau_c\right], \quad (11)$$

where $\mathtt{SINR}_c$ is the signal-to-interference and noise ratio in communication, τ_c is the threshold for decoding in communication which is achieved by the required minimum data rate $r'_{c,com}$, which will be discussed in detail later, $\mathtt{SCNR}_s$ is signal-to-clutter and noise ratio in sensing, τ_s is the threshold for target detection in sensing, $d'_{s,res}$ is the given maximum distance resolution for sensing. We model the locations of BSs, STs, and SCTs using three independent homogeneous Poisson Point Processes (PPPs), with densities γ_{bs}, γ_{st}, and γ_{sct}, respectively.

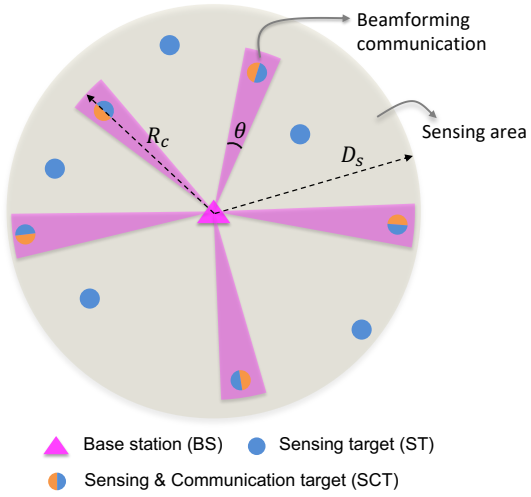

Fig. 3: System model for the JSAC.

B. Interference in the sensing

Considering the interference in sensing, which is elaborated in Fig. 4, on the side of a particular BS, BS_0, which is detecting a tagged ST_0, the interference signal can be classified into three parts: 1) the interference signal coming from other BSs (BS_j in Fig. 4), which can be divided into two parts, direct-path breakthrough signal and import-clutter signal; 2) the interference signal made by other STs ($\mathrm{ST}_i, i = 1, 2, 3, \cdots$, in Fig. 4), which comes from the BS_0, arrive at ST_i, and then reflected again by ST_i to the BS_0, which can be named as the self-clutter signal; 3) clutter signals made by the reflection of the surrounding environment (not highlighted in Fig. 4), like ground, atmospheric gases, rain, etc. Regarding the signal BS_0-ST_i-BS_0, which is the desired signal related to sensing target ST_i at BS_0, it is similar to the blue lines (dash and solid lines, which is the desired signal related to sensing target ST_0 at BS_0) in Fig. 4. In the sensing scenario, distinguishing between different targets (different reflected signals) is related to the multi-target detection performance of FMCW radar. The critical point for the multi-target detection performance is the distance resolution, which is explained in Section II-A, and we will also explore the effect of the distance resolution on the final coverage performance in this paper.

According to the IEEE standards for radar [37], the direct-path breakthrough signal can be filtered by a clutter filter group or filter bank based on the different Doppler shifts. So, we

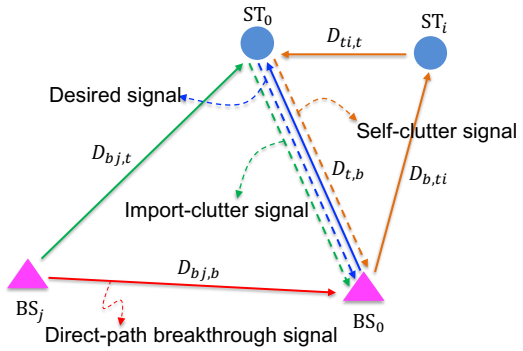

Fig. 4: Interfering model for sensing in JSAC.

can ignore the effects made by the direct-path breakthrough signal. Regarding the difference in the Doppler shifts between the desired signal and the self-clutter signal. Since the moving directions of ST_i and ST_0 are independently random, we can not distinguish the final Doppler shifts in the self-clutter signal and the desired signal. Hence, the self-clutter can not be rejected by the clutter filters, and it will be considered in the analysis. In a small range of detection areas with high densities of BSs and targets, the strength of the clutter caused by the surrounding environment (the third kind of interference) is small compared with the other two types of interference. In this paper, we focus on the first two sources of interferences (named import-clutter and self-clutter) and assume the third one as a given value in dB. Besides that, thermal noise is also considered.

Distances between BS_0 and each interference resource are shown in Fig. 4. Based on the sensing model in (8), we can have interference in the sensing link as

$$\begin{aligned} C_s &= \sum_{j=1,2,\cdots} \left(\frac{P_{s,t} g_{s,t}}{4\pi D_{bj,t}^2} \frac{\rho_{st}}{4\pi D_{t,b}^2} \frac{g_{s,r}\lambda^2}{4\pi} N T_c H_{s,j} \right) \\ &+ \sum_{i=1,2,\cdots} \left(\frac{P_{s,t} g_{s,t}}{4\pi D_{b,ti}^2} \frac{\rho_{st,i}}{4\pi D_{ti,t}^2} \frac{\rho_{st}}{4\pi D_{t,b}^2} \frac{g_{s,r}\lambda^2}{4\pi} N T_c H_{s,i} \right) \\ &\triangleq C_{s,1} + C_{s,2}, \end{aligned} \tag{12}$$

where $H_{s,j}$ and $H_{s,i}$ are channel fading which subject exponential distributions, $C_{s,1}$ indicates the interference caused by the import-clutter signal, and $C_{s,2}$ indicates the interference caused by the self-clutter signal.

C. Adaptive beamwidth in communication

In terms of communication, BS can transmit data to the surrounding SCTs. Since the locations of SCTs are achieved by BS via sensing, beamforming technology can be used while the beam width is indicated as θ. The communication between BS and the SCT is shown in Fig. 5. To ensure that the SCT will be covered by the BS with high energy efficiency, the beamwidth θ is decided by the distance between the SCT and BS, $R_{b,t}$. We assume that all the SCTs will be covered by a coverage diameter C_d. Hence, we can have the relationship between θ, $R_{b,t}$, and C_d as:

$$C_d = 2R_{b,t} \tan(\frac{\theta}{2}) \;\Rightarrow\; \theta = 2 \arctan(\frac{C_d}{2R_{b,t}}). \tag{13}$$

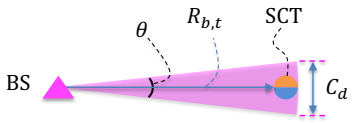

Fig. 5: Beamwidth and cover diameter of the BS.

D. Interference in the communication

Considering commonly used orthogonal multiple access techniques such as time division or frequency division, we assume no interference between different links related to different SCTs that are connected to the same tagged BS. On the side of SCTs, the interference comes from other BSs, and we know that all the interfering BSs are further than the tagged BS to the SCT.

The interference model in communication is shown in Fig. 6, BS_0 is communicating with its desired target SCT_0, and BS_j is communicating with its desired target $\text{SCT}_j, j = 1, 2, 3, \cdots$. All the BSs have their own beamwidth, indicated as θ or θ_j, based on their desired communication distance $R_{b,t}$ or $R_{bj,tj}$. Since all the targets will build communication links with the nearest BS, we have $R_{b,t} < R_{bj,t}$, where $R_{bj,t}$ is the distance between SCT_0 and the interfering BS, BS_j. Based on (13), we can have the expression of the beamwidth of BS_j as $\theta_j = 2\arctan(\frac{C_d}{2R_{bj,tj}})$.

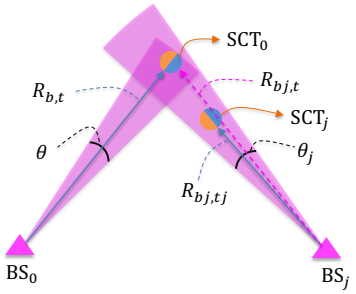

Fig. 6: Interfering model for communication in JSAC.

Based on the structure in Fig. 6, we can have the interference probability of BS_j, which is the probability of the signal transmitted from BS_j to its desired target SCT_j causing an interference at SCT_0, shown as:

$$A_{c,j} = \frac{\theta_j}{2\pi} = \frac{\arctan(\frac{C_d}{2R_{bj,tj}})}{\pi}, \tag{14}$$

where θ_j is the beamwidth of the j-th interfering BS. Hence, we can have interference in the communication link as

$$I_c = \sum_{j=1,2,\cdots} P_{c,r,j}(R_{bj,t}), \tag{15}$$

where $P_{c,r,j}(R_{bj,t})$ is the received interference power of the j-th interfering BS, which is a function of the distance between the interfering BS, BS_j, and SCT_0 and will be discussed in detail later.

E. Allocation of energy and spectrum between sensing and communication

Constrained by the total transmit power P_t and bandwidth B, the trade-off of the two resources must be considered in the joint analysis of JSAC. In this paper, two independent parameters are set to describe the allocation of P&S. We have

$$\begin{cases} P_t &= P_{s,t} + P_{c,t} = \eta P_t + (1-\eta)P_t \\ B &= B_s + B_c = \mu B + (1-\mu)B \end{cases}, \tag{16}$$

where B_s and $P_{s,t}$ are the allocated bandwidth and transmit power for sensing, respectively, and B_c and $P_{c,t}$ are the allocated bandwidth and transmit power for communication, respectively. Regarding the spectrum allocation, the first μB part of the bandwidth will be allocated to sensing, and the remaining part will be used for communication.

IV. Coverage Probability in Joint Sensing and Communication

We introduced the joint CP of JSAC in (11), which will be derived in Theorem 3 later in this section. But first, it is required to compute the CP separately for each sensing and communication as an intermediate step to compute (14). The separate CPs of sensing and communication are given as:

$$P_{s,\text{cov}} = \mathbb{P}[\text{SCNR}_s > \tau_s], \quad P_{c,\text{cov}} = \mathbb{P}[\text{SINR}_c > \tau_c]. \tag{17}$$

A. Analysis of the sensing link

Considering the model introduced in Section II, we can have

$$\begin{aligned}
P_{s,\text{cov}} &= \mathbb{P}[\text{SCNR}_s > \tau_s] = \mathbb{P}\big[\frac{P_{s,r}(D_{t,b})}{C_s + KT_0B_sF_n} > \tau_s\big] \\
&= \mathbb{P}\big[\frac{\frac{P_{s,t}g_{s,t}}{4\pi D_{t,b}^2}\frac{\rho_{st}}{4\pi D_{t,b}^2}\frac{g_{s,r}c^2}{4\pi f_s^2}NT_cH_s}{C_s + KT_0B_sF_n} > \tau_s\big] \\
&= \mathbb{E}_{D_{t,b}}\Big[\mathbb{P}\big[\frac{\frac{P_{s,t}g_{s,t}}{4\pi D_{t,b}^2}\frac{\rho_{st}}{4\pi D_{t,b}^2}\frac{g_{s,r}c^2}{4\pi f_s^2}NT_cH_s}{C_s + KT_0B_sF_n} > \tau_s \big| D_{t,b} = d_{t,b}\big]\Big] \\
&= \int_0^{d_{t,b}^{\max}} \mathbb{P}\big[\frac{\frac{P_{s,t}g_{s,t}}{4\pi d_{t,b}^2}\frac{\rho_{st}}{4\pi d_{t,b}^2}\frac{g_{s,r}c^2}{4\pi f_s^2}NT_cH_s}{C_s + KT_0B_sF_n} > \tau_s \big| D_{t,b} = d_{t,b}\big] \\
&\times f_{D_{t,b}}(d_{t,b})\mathrm{d}d_{t,b} \\
&\overset{(a)}{=} \int_0^{d_{t,b}^{\max}} \mathbb{P}\big[H_s > \frac{\tau_s(C_s + KT_0B_sF_n)}{\frac{P_{s,t}g_{s,t}g_{s,r}\rho_{st}c^2}{(4\pi)^3 f_s^2} d_{t,b}^{-4} NT_c} \big| D_{t,b} = d_{t,b}\big] \\
&\times 2\pi\gamma_{bs}d_{t,b}\exp(-\pi\gamma_{bs}d_{t,b}^2)\mathrm{d}d_{t,b},
\end{aligned} \tag{18}$$

where step (a) results from the well-known contact distance distribution of PPP [38], [39], which gives the PDF of the nearest distance in the homogeneous PPP as $f_{D_{t,b}}(d_{t,b}) = 2\pi\gamma_{bs}D_{t,b}\exp(-\pi\gamma_{bs}d_{t,b}^2)$, $P_{s,t}$ is the transmit power for sensing, $D_{t,b}$ is the distance between ST_0 and BS_0, $g_{s,t}$ and $g_{s,r}$ are gains of the transmitting and the receiving antennas, $c = 3\times10^8$ m/s is the light speed, ρ_{st} is the radar cross section (RCS) on the ST, f_s is the center frequency of chirp ramp, N is the number of the transmitted chirps in a frame, T_c is the duration time of the chirp which is made by the FMCW radar, K is the Boltzmann constant, T_0 is the standard temperature, B_s is the bandwidth for sensing, F_n is the noise figure, C_s is the total clutter signal power given in (12), τ_s is the threshold for the target sensing.

Remark 1. *Based on the derivation in (18), we can see that if the bandwidth allocated to sensing increases, the sensing CP will decrease; if the power allocated to sensing increases,*

the sensing CP will be improved. For instance, from the perspective of energy resources, communication and sensing compete with each other, but there is no competition for bandwidth resources (communication hopes to obtain more bandwidth). However, more constraints will be given by the requirement of distance resolution later, and more remarks will be given. Furthermore, all of them will be revealed in the simulation section.

Given that $H_s \sim \exp(1)$, the inner probability term of (18) can be further simplified as

$$\begin{aligned}
&\mathbb{P}\big[H_s > \frac{\tau_s(C_s + KT_0B_sF_n)}{\frac{P_{s,t}g_{s,t}g_{s,r}\rho_{st}c^2}{(4\pi)^3 f_s^2} d_{t,b}^{-4} NT_c} \big| d_{t,b}\big] \\
&= \mathbb{E}_{C_s}\Big[\mathbb{P}\big[H_s > \frac{\tau_s(C_s + KT_0B_sF_n)}{\frac{P_{s,t}g_{s,t}g_{s,r}\rho_{st}c^2}{(4\pi)^3 f_s^2} d_{t,b}^{-4} NT_c} \big| C_s, d_{t,b}\big]\Big] \\
&= \mathbb{E}_{C_s}\big[\exp\big(-\tau_s(C_s + KT_0B_sF_n) \\
&\times (P_{s,t}g_{s,t}g_{s,r}\rho_{st}c^2NT_c)^{-1}(4\pi)^3 f_s^2 d_{t,b}^4\big)\big] \\
&= \mathbb{E}_{C_{s,1},C_{s,2}}\big[\exp\big(-\tau_s(C_{s,1} + C_{s,2} + KT_0B_sF_n) \\
&\times (P_{s,t}g_{s,t}g_{s,r}\rho_{st}c^2NT_c)^{-1}(4\pi)^3 f_s^2 d_{t,b}^4\big)\big] \\
&= \exp\big(-\tau_s KT_0B_sF_n(P_{s,t}g_{s,t}g_{s,r}\rho_{st}c^2NT_c)^{-1} \\
&\times (4\pi)^3 f_s^2 d_{t,b}^4)\mathbb{E}_{C_{s,1}}\big[\exp\big(-\tau_s C_{s,1} \\
&\times (P_{s,t}g_{s,t}g_{s,r}\rho_{st}c^2NT_c)^{-1}(4\pi)^3 f_s^2 d_{t,b}^4\big)\big] \\
&\times \mathbb{E}_{C_{s,2}}\big[\exp\big(-\tau_s C_{s,2}(P_{s,t}g_{s,t}g_{s,r}\rho_{st}c^2NT_c)^{-1}(4\pi)^3 f_s^2 d_{t,b}^4\big)\big] \\
&= \exp\big(-\tau_s KT_0B_sF_n(P_{s,t}g_{s,t}g_{s,r}\rho_{st}c^2NT_c)^{-1}(4\pi)^3 \\
&\times f_s^2 d_{t,b}^4)\mathcal{L}_{C_{s,1}}\big(\tau_s(P_{s,t}g_{s,t}g_{s,r}\rho_{st}c^2NT_c)^{-1}(4\pi)^3 f_s^2 d_{t,b}^4\big) \\
&\times \mathcal{L}_{C_{s,2}}\big(\tau_s(P_{s,t}g_{s,t}g_{s,r}\rho_{st}c^2NT_c)^{-1}(4\pi)^3 f_s^2 d_{t,b}^4\big), \qquad (19)
\end{aligned}$$

where $\mathcal{L}_{C_{s,1}}(\cdot)$ and $\mathcal{L}_{C_{s,2}}(\cdot)$ are the clutter Laplace transforms, which are computed in the following lines.

In the following, we will calculate the Laplace transform of $C_{s,1}$ and $C_{s,2}$ separately ($C_{s,1}$ and $C_{s,2}$ are shown in (12)).

1) Laplace transform of $C_{s,1}$:

$$\begin{aligned}
&\mathcal{L}_{C_{s,1}}(s) = \mathbb{E}\big[\exp(-sC_{s,1})\big|D_{t,b} = d_{t,b}\big] \\
&= \mathbb{E}\big[\exp\big(-s\sum_{j=1,2,\cdots}(\frac{P_{s,t}g_{s,t}}{4\pi D_{bj,t}^2}\frac{\rho_{st}}{4\pi D_{t,b}^2}\frac{g_{s,r}\lambda^2}{4\pi} \\
&\times NT_cH_{s,j})\big)\big|D_{t,b} = d_{t,b}\big] \\
&= \mathbb{E}\big[\prod_{j=1,2,\cdots}\exp\big(-s\frac{P_{s,t}g_{s,t}}{4\pi D_{bj,t}^2}\frac{\rho_{st}}{4\pi D_{t,b}^2}\frac{g_{s,r}\lambda^2}{4\pi} \\
&\times NT_cH_{s,j}\big)\big|D_{t,b} = d_{t,b}\big].
\end{aligned}$$

Based on the fact that $H_{s,j}, j = 1, 2, \cdots$ are independent, we can move the expectation with respect to $H_{s,j}$ inside the multiplication, and we can have

$$\begin{aligned}
&\mathcal{L}_{C_{s,1}}(s) = \mathbb{E}\Big[\prod_{j=1,2,\cdots}\mathbb{E}_{H_{s,j}}\big[\exp\big(-s\frac{P_{s,t}g_{s,t}}{4\pi D_{bj,t}^2} \\
&\times \frac{\rho_{st}}{4\pi D_{t,b}^2}\frac{g_{s,r}\lambda^2}{4\pi}NT_cH_{s,j}\big)\big|D_{t,b} = d_{t,b}\big]\Big] \\
&\overset{(b)}{=} \exp\big(-\gamma_{bs}\int_{\mathbb{R}^2}\big(1 - \mathbb{E}_{H_{s,j}}\big[\exp(-s\frac{P_{s,t}g_{s,t}}{4\pi d_{bj,t}^2} \\
&\times \frac{\rho_{st}}{4\pi D_{t,b}^2}\frac{g_{s,r}\lambda^2}{4\pi}NT_cH_{s,j}\big)\big|D_{t,b} = d_{t,b}\big]\big)\mathrm{d}\mathbf{x}\big),
\end{aligned}$$

where step (b) results from applying probability generating functional (PGFL) of PPP [38], and $\mathbf{x}$ is the locations of the interfering BSs, BS_j.

Since we know that the distance between the BS_j and ST_0 is bigger than the distance between BS_0 and ST_0, $D_{bj,t} \geq D_{b,t}$. Employing a transformation to polar coordinates, we can get

$$\begin{aligned}
&\mathcal{L}_{C_{s,1}}(s) = \exp\big(-2\pi\gamma_{bs}\int_{d_{b,t}}^{d_{bj,t}^{\max}}\big(1 - \mathbb{E}_{H_{s,j}}\big[\exp(-s \\
&\times \frac{P_{s,t}g_{s,t}}{4\pi d_{bj,t}^2}\frac{\rho_{st}}{4\pi d_{t,b}^2}\frac{g_{s,r}\lambda^2}{4\pi}NT_cH_{s,j})\big|d_{t,b}\big]\big)d_{bj,t}\mathrm{d}d_{bj,t}\big) \\
&\overset{(c)}{=} \exp\big(-2\pi\gamma_{bs}\int_{d_{b,t}}^{d_{bj,t}^{\max}}(1 \\
&- \frac{1}{1 + s\frac{P_{s,t}g_{s,t}}{4\pi d_{bj,t}^2}\frac{\rho_{st}}{4\pi d_{t,b}^2}\frac{g_{s,r}\lambda^2}{4\pi}NT_c})\times d_{bj,t}\mathrm{d}d_{bj,t}\big) \\
&= \exp\big(-2\pi\gamma_{bs} \\
&\times \int_{d_{b,t}}^{d_{bj,t}^{\max}}(\frac{1}{1 + s^{-1}(\frac{P_{s,t}g_{s,t}}{4\pi d_{bj,t}^2}\frac{\rho_{st}}{4\pi d_{t,b}^2}\frac{g_{s,r}\lambda^2}{4\pi}NT_c)^{-1}})d_{bj,t}\mathrm{d}d_{bj,t}\big),
\end{aligned}$$

where step (c) follows from the fact that $H_{s,j}$ is exponentially distributed, and $d_{bj,t}^{\max}$ is the maximum communication distance for the outdoor short-range field as described before (9). Hence, we can have the Laplace transform of $C_{s,1}$ in (19),

$$\begin{aligned}
&\mathcal{L}_{C_{s,1}}\big(\tau_s(P_{s,t}g_{s,t}g_{s,r}\rho_{st}c^2NT_c)^{-1}(4\pi)^3 f_s^2 d_{t,b}^4\big) \\
&= \exp\big(-2\pi\gamma_{bs}\int_{d_{b,t}}^{d_{bj,t}^{\max}}(\frac{\tau_s}{\tau_s + (\frac{d_{bj,t}}{d_{t,b}})^2})d_{bj,t}\mathrm{d}d_{bj,t}\big). \qquad (20)
\end{aligned}$$

2) Laplace transform of $C_{s,2}$:

$$\begin{aligned}
&\mathcal{L}_{C_{s,2}}(s) = \mathbb{E}\big[\exp(-sC_{s,2})\big|D_{t,b} = d_{t,b}\big] \\
&= \mathbb{E}\big[\exp\big(-s\sum_{i=1,2,\cdots}(\frac{P_{s,t}g_{s,t}}{4\pi D_{b,ti}^2}\frac{\rho_{st,i}}{4\pi D_{ti,t}^2}\frac{\rho_{st}}{4\pi D_{t,b}^2}\frac{g_{s,r}\lambda^2}{4\pi} \\
&\times NT_cH_{s,i})\big)\big|D_{t,b} = d_{t,b}\big] \\
&= \mathbb{E}\big[\prod_{i=1,2,\cdots}\exp(-s\frac{P_{s,t}g_{s,t}}{4\pi D_{b,ti}^2}\frac{\rho_{st,i}}{4\pi D_{ti,t}^2}\frac{\rho_{st}}{4\pi D_{t,b}^2}\frac{g_{s,r}\lambda^2}{4\pi} \\
&\times NT_cH_{s,i})\big|D_{t,b} = d_{t,b}\big]. \qquad (21)
\end{aligned}$$

Based on the fact that $H_{s,i}, i = 1, 2, \cdots$ are independent, we can move the expectation with respect to $H_{s,i}$ inside the multiplication, and we can have

$$\begin{aligned}
&\mathcal{L}_{C_{s,2}}(s) = \mathbb{E}\Big[\prod_{i=1,2,\cdots}\mathbb{E}_{H_{s,i}}\big[\exp(-s\frac{P_{s,t}g_{s,t}}{4\pi D_{b,ti}^2}\frac{\rho_{st,i}}{4\pi D_{ti,t}^2} \\
&\times \frac{\rho_{st}}{4\pi D_{t,b}^2}\frac{g_{s,r}\lambda^2}{4\pi}NT_cH_{s,i})\big|D_{t,b} = d_{t,b}\big]\Big].
\end{aligned}$$

As shown in Fig. 7, we can have the relationship between $D_{b,ti}$, $D_{ti,t}$, and $D_{t,b}$ as

$$D_{b,ti}^2 = D_{t,b}^2 + D_{ti,t}^2 - 2D_{t,b}D_{ti,t}\cos(\psi), \qquad (22)$$

where $D_{t,b}$ and ψ are independent and $f_{D_{t,b}}(d_{t,b}) = 2\pi\gamma_{bs}d_{t,b}\exp(-\pi\gamma_{bs}d_{t,b}^2)$, $f(\psi) = \frac{1}{2\pi}$, $0 \leq \psi \leq 2\pi$.

Hence, we can have

$$\begin{aligned}
&\mathcal{L}_{C_{s,2}}(s) = \mathbb{E}\Big[\prod_{i=1,2,\cdots}\mathbb{E}_{H_{s,i}}\big[\exp(-s \\
&\times \frac{P_{s,t}g_{s,t}}{4\pi(d_{t,b}^2 + D_{ti,t}^2 - 2d_{t,b}D_{ti,t}\cos(\psi))}
\end{aligned}$$

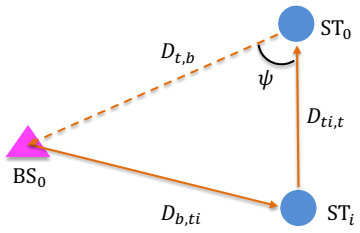

Fig. 7: Relationships between $D_{b,ti}$, $D_{ti,t}$, $D_{t,b}$, and ψ.

$$\times \frac{\rho_{st,i}}{4\pi D_{ti,t}^2}\frac{\rho_{st}}{4\pi d_{t,b}^2}\frac{g_{s,r}\lambda^2}{4\pi}NT_cH_{s,i})\big|d_{t,b}\big]\Big]$$
$$\overset{(d)}{=} \exp\Big(-\gamma_{st}$$
$$\times \int_{\mathbb{R}^2}\big(1-\mathbb{E}_{H_{s,i}}\big[\exp(\frac{-sP_{s,t}g_{s,t}}{4\pi(d_{t,b}^2+d_{ti,t}^2-2d_{t,b}d_{ti,t}\cos(\psi))}$$
$$\times \frac{\rho_{st,i}}{4\pi d_{ti,t}^2}\frac{\rho_{st}}{4\pi d_{t,b}^2}\frac{g_{s,r}\lambda^2}{4\pi}NT_cH_{s,i})\big|d_{t,b}\big]\big)\mathrm{d}\mathbf{x}\Big) = (e),$$

where step (d) applying PGFL of PPP [38], $\mathbf{x}$ is the locations of the STs involved in self-clutter, ST_i, and $d_{ti,t}^{\max}$ is the maximum communication distance for outdoor short-range field as described before (9), step (e) is calculated in (24) (at the top of next page). In (24), step(f) results from the exponential function. Hence, we can have the Laplace transform of $C_{s,2}$,

$$\mathcal{L}_{C_{s,2}}(\tau_s(P_{s,t}g_{s,t}g_{s,r}\rho_{st}c^2NT_c)^{-1}(4\pi)^3f_s^2d_{t,b}^4)$$
$$= \exp\Big(-\gamma_{st}\int_0^{2\pi}\int_0^{d_{ti,t}^{\max}}$$
$$\times\big(\frac{\tau_s}{\tau_s+\frac{4\pi d_{ti,t}^2(d_{t,b}^2+d_{ti,t}^2-2d_{t,b}d_{ti,t}\cos(\psi))}{\rho_{st,i}d_{t,b}^2}}\big)d_{ti,t}\mathrm{d}d_{ti,t}\mathrm{d}\psi\Big). \tag{23}$$

Using the Laplace transform over $C_{s,1}$ and $C_{s,2}$ in (20) and (23), we can calculate (19) as

$$\mathbb{P}\big[H_s > \frac{\tau_s(C_s+KT_0B_sF_n)}{\frac{P_{s,t}g_{s,t}g_{s,r}\rho_{st}c^2}{(4\pi)^3f_s^2}d_{t,b}^{-4}NT_c}\big|d_{t,b}\big]$$
$$= \exp\big(-\tau_sKT_0B_sF_n(P_{s,t}g_{s,t}g_{s,r}\rho_{st}c^2NT_c)^{-1}(4\pi)^3f_s^2d_{t,b}^4\big)$$
$$\times \exp\big(-2\pi\gamma_{bs}\int_{d_{b,t}}^{d_{bj,t}^{\max}}\big(\frac{\tau_s}{\tau_s+(\frac{d_{bj,t}}{d_{t,b}})^2}\big)d_{bj,t}\mathrm{d}d_{bj,t}\big)\exp\big(-\gamma_{st}\int_0^{2\pi}$$
$$\times\int_0^{d_{ti,t}^{\max}}\big(\frac{\tau_s}{\tau_s+\frac{4\pi d_{ti,t}^2(d_{t,b}^2+d_{ti,t}^2-2d_{t,b}d_{ti,t}\cos(\psi))}{\rho_{st,i}d_{t,b}^2}}\big)d_{ti,t}\mathrm{d}d_{ti,t}\mathrm{d}\psi\big). \tag{27}$$

Substituting for (27) into (18), we can have the final expression of the CP of the sensing link in JSAC.

Theorem 1. *The probability of sensing coverage in JSAC is*

$$P_{s,\mathrm{cov}} = \mathbb{P}[\mathtt{SCNR}_s > \tau_s] = \int_0^{d_{t,b}^{\max}}\mathbb{P}\big[H_s > \frac{\tau_s}{\frac{P_{s,t}g_{s,t}g_{s,r}\rho_{st}c^2}{(4\pi)^3f_s^2}}$$
$$\times\frac{(C_s+KT_0B_sF_n)}{d_{t,b}^{-4}NT_c}\big]2\pi\gamma_{bs}d_{t,b}\exp(-\pi\gamma_{bs}d_{t,b}^2)\mathrm{d}d_{t,b}$$
$$= \int_0^{d_{t,b}^{\max}}\Big(\exp(-\tau_sKT_0B_sF_n(P_{s,t}g_{s,t}g_{s,r}\rho_{st}c^2NT_c)^{-1}(4\pi)^3$$
$$\times f_s^2d_{t,b}^4)\exp\big(-2\pi\gamma_{bs}\int_{d_{b,t}}^{d_{bj,t}^{\max}}\big(\frac{\tau_s}{\tau_s+(\frac{d_{bj,t}}{d_{t,b}})^2}\big)d_{bj,t}\mathrm{d}d_{bj,t}\big)$$
$$\times\exp\big(-\gamma_{st}\int_0^{2\pi}\int_0^{d_{ti,t}^{\max}}\big(\frac{\tau_s}{\tau_s+\frac{4\pi d_{ti,t}^2(d_{t,b}^2+d_{ti,t}^2-2d_{t,b}d_{ti,t}\cos(\psi))}{\rho_{st,i}d_{t,b}^2}}\big)$$
$$\times d_{ti,t}\mathrm{d}d_{ti,t}\mathrm{d}\psi\big)\times 2\pi\gamma_{bs}d_{t,b}\exp(-\pi\gamma_{bs}d_{t,b}^2)\Big)\mathrm{d}d_{t,b}. \tag{28}$$

B. Analysis of the communication link

Based on the communication channel in (10), the CP of the communication in JSAC between the tagged BS_0 and the target SCT_0 at a random distance $R_{b,t}$ is

$$P_{c,\mathrm{cov}} = \mathbb{P}[\mathtt{SINR}_c > \tau_c]$$
$$= \mathbb{P}\big[\frac{P_{c,r}(R_{b,t})}{N_0B_c+I_c} > \tau_c\big] = \mathbb{P}\big[\frac{\frac{P_{c,t}\times 10^{2.8}}{f_c^2R_{b,t}^{1.9}\times 10^{0.1L_s}}H_cg_{c,b}}{N_0B_c+I_c} > \tau_c\big]$$
$$= \mathbb{E}_{R_{b,t}}\Big[\mathbb{P}\big[\frac{\frac{P_{c,t}\times 10^{2.8}}{f_c^2R_{b,t}^{1.9}\times 10^{0.1L_s}}H_cg_{c,b}}{N_0B_c+I_c} > \tau_c\big|R_{b,t}=r_{b,t}\big]\Big]$$
$$= \int_0^{r_{b,t}^{\max}}\mathbb{P}\big[\frac{\frac{P_{c,t}10^{2.8}}{f_c^2r_{b,t}^{1.9}10^{0.1L_s}}H_cg_{c,b}}{N_0B_c+I_c} > \tau_c\big|r_{b,t}\big]f_{R_{b,t}}(r_{b,t})\mathrm{d}r_{b,t}$$
$$= \int_0^{r_{b,t}^{\max}}\mathbb{P}\big[H_c > \tau_c(N_0B_c+I_c)f_c^2r_{b,t}^{1.9}$$
$$\times P_{c,t}^{-1}g_{c,b}^{-1}10^{(0.1L_s-2.8)}\big|r_{b,t}\big]f_{R_{b,t}}(r_{b,t})\mathrm{d}r_{b,t}, \tag{29}$$

where $r_{b,t}^{\max}$ is the maximum communication distance for the outdoor short-range field as described before (9), $P_{c,t}$ is the transmit power of communication, $R_{b,t}$ is the distance between BS_0 and SCT_0, which is the nearest distance in PPP and $f_{R_{b,t}}(r_{b,t}) = 2\pi\gamma_{bs}r_{b,t}\exp(-\pi\gamma_{bs}r_{b,t}^2)$, H_c is the exponentially distributed fading gain of the channel, $g_{c,b} = 10^{0.1G_{c,b}}$ where $G_{c,b}$ is the beamforming gain of communication in dB, f_c is the center frequency, N_0 is the power spectral density of noise in communication, B_c is the bandwidth used for communication, I_c is the total interference power, τ_c is the minimum required SINR threshold to ensure successful connection.

Remark 2. *The communication model is more like a cellular network rather than an ad-hoc network. The end-user will communicate with the nearest BS. Shown as the second line in (29), we can see that when the density of BS γ_{bs} increases, the total interference I_c will increase. Meanwhile, the communication distance between the BS and end-user decreases, which is also indicated in the distribution of the communication distance, $f_{R_{b,t}}(r_{b,t}) = 2\pi\gamma_{bs}r_{b,t}\exp(-\pi\gamma_{bs}r_{b,t}^2)$. Hence, we can expect that the communication coverage probability will not reach 0 asymptotically as the density γ_{bs} goes to infinity, which will also be revealed in the simulation part.*

Given the fact that $H_c \sim \exp(1)$, the inner probability term of (29) can be further simplified as

$$\mathbb{P}\big[H_c > \tau_c(N_0B_c+I_c)f_c^2r_{b,t}^{1.9}P_{c,t}^{-1}g_{c,b}^{-1}10^{(0.1L_s-2.8)}\big|r_{b,t}\big]$$
$$= \mathbb{E}_{I_c}\big[\mathbb{P}[H_c > \tau_c(N_0B_c+I_c)f_c^2r_{b,t}^{1.9}$$
$$\times P_{c,t}^{-1}g_{c,b}^{-1}10^{(0.1L_s-2.8)}\big|I_c,r_{b,t}\big]\big]$$
$$= \mathbb{E}_{I_c}\big[\exp\big(-\tau_c(N_0B_c+I_c)f_c^2r_{b,t}^{1.9}$$

$$(e)=\exp\big(-\gamma_{st}\int_0^{2\pi}\int_0^{d_{ti,t}^{\max}}\big(1-\mathbb{E}_{H_{s,i}}\big[\exp(\frac{-sP_{s,t}g_{s,t}NT_cH_{s,i}}{4\pi(d_{t,b}^2+d_{ti,t}^2-2d_{t,b}d_{ti,t}\cos(\psi))}\frac{\rho_{st,i}}{4\pi d_{ti,t}^2}\frac{\rho_{st}}{4\pi d_{t,b}^2}\frac{g_{s,r}\lambda^2}{4\pi})\big|d_{t,b}\big]\big)d_{ti,t}\mathrm{d}d_{ti,t}\mathrm{d}\psi\big) \quad (24)$$

$$\overset{(f)}{=}\exp\big(-\gamma_{st}\int_0^{2\pi}\int_0^{d_{ti,t}^{\max}}\big(1-\frac{1}{1+s\times\frac{P_{s,t}g_{s,t}}{4\pi(d_{t,b}^2+d_{ti,t}^2-2d_{t,b}d_{ti,t}\cos(\psi))}\frac{\rho_{st,i}}{4\pi d_{ti,t}^2}\frac{\rho_{st}}{4\pi d_{t,b}^2}\frac{g_{s,r}\lambda^2}{4\pi}NT_c}\big)d_{ti,t}\mathrm{d}d_{ti,t}\mathrm{d}\psi\big) \quad (25)$$

$$=\exp\big(-\gamma_{st}\int_0^{2\pi}\int_0^{d_{ti,t}^{\max}}\big(\frac{1}{1+s^{-1}\times(\frac{P_{s,t}g_{s,t}}{4\pi(d_{t,b}^2+d_{ti,t}^2-2d_{t,b}d_{ti,t}\cos(\psi))}\frac{\rho_{st,i}}{4\pi d_{ti,t}^2}\frac{\rho_{st}}{4\pi d_{t,b}^2}\frac{g_{s,r}\lambda^2}{4\pi}NT_c)^{-1}}\big)d_{ti,t}\mathrm{d}d_{ti,t}\mathrm{d}\psi\big). \quad (26)$$

$$\times P_{c,t}^{-1}g_{c,b}^{-1}10^{(0.1L_s-2.8)}\big)\big|r_{b,t}\big]$$
$$=\exp\big(-\tau_cN_0B_cf_c^2r_{b,t}^{1.9}P_{c,t}^{-1}g_{c,b}^{-1}10^{(0.1L_s-2.8)}\big)$$
$$\times\mathbb{E}_{I_c}\big[\exp\big(-\tau_cI_cf_c^2r_{b,t}^{1.9}P_{c,t}^{-1}g_{c,b}^{-1}10^{(0.1L_s-2.8)}\big)\big]$$
$$=\exp\big(-\tau_cN_0B_cf_c^2r_{b,t}^{1.9}P_{c,t}^{-1}g_{c,b}^{-1}10^{(0.1L_s-2.8)}\big)$$
$$\times\mathcal{L}_{I_c}\big(\tau_cf_c^2r_{b,t}^{1.9}P_{c,t}^{-1}g_{c,b}^{-1}10^{(0.1L_s-2.8)}\big), \quad (30)$$

where $\mathcal{L}_{I_c}(\cdot)$ is the interference Laplace transform, which is computed as follows.

Based on the communication channel in (10), we can have

$$I_c=\sum_{j=1,2,\cdots}P_{c,r,j}(R_{bj,t})=\sum_{j=1,2,\cdots}\frac{P_{c,t}10^{2.8}H_{c,j}g_{c,b}}{f_c^2R_{bj,t}^{1.9}10^{0.1L_s}}$$
$$=\sum_{j=1,2,\cdots}10^{(2.8-0.1L_s)}P_{c,t}f_c^{-2}R_{bj,t}^{-1.9}H_{c,j}g_{c,b}. \quad (31)$$

Computing the Laplace transform of I_c, we get

$$\mathcal{L}_{I_c}(s)=\mathbb{E}[\exp(-sI_c)]$$
$$=\mathbb{E}\Big[\exp\big(-s\sum_{j=1,2,\cdots}10^{(2.8-0.1L_s)}P_{c,t}f_c^{-2}R_{bj,t}^{-1.9}H_{c,j}g_{c,b}\big)\Big]$$
$$=\mathbb{E}\big[\prod_{j=1,2,\cdots}\exp\big(-s10^{(2.8-0.1L_s)}P_{c,t}f_c^{-2}R_{bj,t}^{-1.9}H_{c,j}g_{c,b}\big)\big].$$

Based on the fact that $H_{c,j}, j=1,2,\cdots$ are independent, we can move the expectation with respect to $H_{c,j}$ inside the multiplication, and we can have

$$\mathcal{L}_{I_c}(s)=\mathbb{E}\Big[\prod_{j=1,2,\cdots}\mathbb{E}_{H_c}\big[\exp(-s10^{(2.8-0.1L_s)}$$
$$\times P_{c,t}f_c^{-2}R_{bj,t}^{-1.9}H_cg_{c,b})\big]\Big]. \quad (32)$$

Considering the fact that each BS has an interfering probability with SCT_0 of $A_{c,j}$ (due to beamforming) and applying PGFL of PPP, we get

$$\mathcal{L}_{I_c}(s)\overset{(g)}{=}\exp\big(-\gamma_{bs}A_{c,j}\int_{\mathbb{R}^2}\big(1-\mathbb{E}_{H_c}\big[\exp(-s$$
$$\times10^{(2.8-0.1L_s)}P_{c,t}f_c^{-2}r_{bj,t}^{-1.9}H_cg_{c,b})\big]\big)\mathrm{d}\mathbf{x}\big),$$

where step (g) results from applying PGFL of PPP [38], and $\mathbf{x}$ is the locations of the interfering base stations, BS_j.

Since we know that the distance between the BS_j and SCT_0 is bigger than the distance between BS_0 and SCT_0, $R_{bj,t}\geq R_{b,t}$. Employing a transformation to polar coordinates, we can get

$$\mathcal{L}_{I_c}(s)=\exp\big(-2\pi\gamma_{bs}A_{c,j}\int_{r_{b,t}}^{r_{bj,t}^{\max}}\big(1-\mathbb{E}_{H_c}\big[\exp(-s$$
$$\times10^{2.8-0.1L_s}P_{c,t}f_c^{-2}r_{bj,t}^{-1.9}H_cg_{c,b})\big]\big)r_{bj,t}\mathrm{d}r_{bj,t}\big),$$

where $r_{bj,t}^{\max}$ is the maximum communication distance for the outdoor short-range field as described before (9). Since $H_{c,j}\sim\exp(1)$, the moment generating function of an exponential random variable can be applied, and $\mathcal{L}_{I_c}(s)$ can be calculated as

$$\mathcal{L}_{I_c}(s)=\exp\big(-2\pi\gamma_{bs}A_{c,j}\int_{r_{b,t}}^{r_{bj,t}^{\max}}\big(1-\mathbb{E}_{H_c}\big[\exp(-s$$
$$\times10^{2.8-0.1L_s}P_{c,t}f_c^{-2}r_{bj,t}^{-1.9}H_cg_{c,b})\big]\big)r_{bj,t}\mathrm{d}r_{bj,t}\big)$$
$$\overset{(h)}{=}\exp\big(-2\pi\gamma_{bs}A_{c,j}\int_{r_{b,t}}^{r_{bj,t}^{\max}}$$
$$\times(1-\frac{1}{1+s10^{2.8-0.1L_s}P_{c,t}f_c^{-2}r_{bj,t}^{-1.9}g_{c,b}})r_{bj,t}\mathrm{d}r_{bj,t}\big)$$
$$=\exp\big(-2\pi\gamma_{bs}A_{c,j}$$
$$\times\int_{r_{b,t}}^{r_{bj,t}^{\max}}\frac{r_{bj,t}}{1+s^{-1}(10^{2.8-0.1L_s}P_{c,t}f_c^{-2}r_{bj,t}^{-1.9}g_{c,b})^{-1}}\mathrm{d}r_{bj,t}\big), \quad (33)$$

where step (h) follows from the fact that H_c is exponentially distributed. Hence, we can have the Laplace transform of I_c in (30) as

$$\mathcal{L}_{I_c}\big(\tau_cf_c^2r_{b,t}^{1.9}P_{c,t}^{-1}g_{c,b}^{-1}10^{(0.1L_s-2.8)}\big)$$
$$=\exp\big(-2\pi\gamma_{bs}A_{c,j}\int_{r_{b,t}}^{r_{bj,t}^{\max}}(\frac{\tau_c}{\tau_c+(\frac{r_{bj,t}}{r_{b,t}})^{1.9}})r_{bj,t}\mathrm{d}r_{bj,t}\big).$$

With the Laplace transform of I_c in (33), we can get (30) as

$$\mathbb{P}\big[H_c>\tau_c(N_0B_c+I_c)f_c^2r_{b,t}^{1.9}P_{c,t}^{-1}g_{c,b}^{-1}10^{(0.1L_s-2.8)}\big|r_{b,t}\big]$$
$$=\exp\big(-\tau_cN_0B_cf_c^2r_{b,t}^{1.9}P_{c,t}^{-1}g_{c,b}^{-1}10^{(0.1L_s-2.8)}\big)$$
$$\times\mathcal{L}_{I_c}\big(\tau_cf_c^2r_{b,t}^{1.9}P_{c,t}^{-1}g_{c,b}^{-1}10^{(0.1L_s-2.8)}\big)$$
$$=\exp\big(-\tau_cN_0B_cf_c^2r_{b,t}^{1.9}P_{c,t}^{-1}g_{c,b}^{-1}10^{(0.1L_s-2.8)}\big)$$
$$\times\exp\big(-2\pi\gamma_{bs}A_{c,j}\int_{r_{b,t}}^{r_{bj,t}^{\max}}(\frac{\tau_c}{\tau_c+(\frac{r_{bj,t}}{r_{b,t}})^{1.9}})r_{bj,t}\mathrm{d}r_{bj,t}\big). \quad (34)$$

Taking the interference probability $A_{c,j}$ in (14) into consideration and the expectation over $R_{bj,tj}$, we can have

$$\mathbb{P}\big[H_c>\tau_c(N_0B_c+I_c)f_c^2r_{b,t}^{1.9}P_{c,t}^{-1}g_{c,b}^{-1}10^{(0.1L_s-2.8)}\big|r_{b,t}\big]$$
$$=\exp\big(-\tau_cN_0B_cf_c^2r_{b,t}^{1.9}P_{c,t}^{-1}g_{c,b}^{-1}10^{(0.1L_s-2.8)}\big)$$
$$\times\int_0^{r_{bj,tj}^{\max}}\exp\Big(-2\pi\gamma_{bs}\frac{\arctan(\frac{C_d}{2r_{bj,tj}})}{\pi}$$
$$\times\int_{r_{b,t}}^{r_{bj,t}^{\max}}(\frac{\tau_c}{\tau_c+(\frac{r_{bj,t}}{r_{b,t}})^{1.9}})r_{bj,t}\mathrm{d}r_{bj,t}\Big)f_{R_{bj,tj}}(r_{bj,tj})\mathrm{d}r_{bj,tj},$$

where $f_{R_{bj,tj}}(r_{bj,tj})=2\pi\gamma_{sct}r_{bj,tj}\exp(-\pi\gamma_{sct}r_{bj,tj}^2)$, and $r_{bj,tj}^{\max}$ is the maximum communication distance for outdoor

short-range field as described before (9).

Substituting for (34) into (29), we can have the final expression of the CP of the communication link in JSAC.

Theorem 2. *The communication CP in JSAC is*

$$P_{c,\mathrm{cov}} = \mathbb{P}[\mathtt{SINR}_c > \tau_c] = \int_0^{r_{b,t}^{\max}} \mathbb{P}\big[H_c > \tau_c(N_0 B_c + I_c) f_c^2 \times r_{b,t}^{1.9} P_{c,t}^{-1} g_{c,b}^{-1} 10^{(0.1L_s - 2.8)}\big] 2\pi\gamma_{bs} r_{b,t} \exp(-\pi\gamma_{bs} r_{b,t}^2) \mathrm{d}r_{b,t}$$
$$= \int_0^{r_{b,t}^{\max}} \Bigg(\exp\big(-\tau_c N_0 B_c f_c^2 r_{b,t}^{1.9} P_{c,t}^{-1} g_{c,b}^{-1} 10^{(0.1L_s-2.8)}\big) \times \int_0^{r_{bj,tj}^{\max}} \exp\Big(-2\pi\gamma_{bs} \frac{\arctan(\frac{C_d}{2r_{bj,tj}})}{\pi} \times \int_{r_{b,t}}^{r_{bj,t}^{\max}} \big(\frac{\tau_c}{\tau_c + (\frac{r_{bj,t}}{r_{b,t}})^{1.9}}\big) r_{bj,t} \mathrm{d}r_{bj,t}\Big) f_{R_{bj,tj}}(r_{bj,tj}) \mathrm{d}r_{bj,tj} \times 2\pi\gamma_{bs} r_{b,t} \exp(-\pi\gamma_{bs} r_{b,t}^2)\Bigg) \mathrm{d}r_{b,t}. \quad (35)$$

C. Constraints of SDR and HDR

Considering principle requirements in JSAC, an SDR and an HDR are desired. According to the relationship between power, spectrum, and distance resolution in Section II, we have

$$D_{s,\mathrm{res}} = \frac{cT_c}{2B_s(T_c - \frac{2D_{t,b}}{c})} \le d'_{s,res}$$
$$\Rightarrow D_{t,b} \le \frac{c}{2}(T_c - \frac{cT_c}{2B_s d'_{s,res}}),$$

where $d'_{s,res}$ is the desired SDR in sensing. Considering the requirement of data rate in communication, we will replace the threshold τ_c with a given HDR, $r'_{c,com}$. According to the well-known Shannon-Hartley theorem, we can have

$$r'_{c,com} = B_c \log_2(1+\tau_c) \Rightarrow \tau_c = 2^{\frac{r'_{c,com}}{B_c}} - 1. \quad (36)$$

Remark 3. *As derived in this sub-section, we can find that if the SDR is required, a bigger allocated bandwidth is desired for sensing, which will compete with the communication for bandwidth resources. Besides that, The HDR in communication will also require more bandwidth, which is shown in (36) with a given τ_c.*

D. Joint analysis of JSAC

According to the previous derivation results, considering the constraints of SDR and transforming the decoding threshold in communication τ_c into the constraint of HDR, the final expression of the joint CP in JSAC can be given as follows.

Theorem 3. *The joint CP of JSAC is derived as*

$$\mathbb{P}_{\mathrm{j,cov}} = \int_0^{d'_{t,b}} \Big(\exp(-\tau_s K T_0 B_s F_n (P_{s,t} g_{s,t} g_{s,r} \rho_{st} c^2 N T_c)^{-1} \times (4\pi)^3 f_s^2 d_{t,b}^4) \exp\big(-2\pi\gamma_{bs} \int_{d_{b,t}}^{d_{bj,t}^{\max}} (\frac{\tau_s}{\tau_s + (\frac{d_{bj,t}}{d_{t,b}})^2}) d_{bj,t} \mathrm{d}d_{bj,t}\big)$$
$$\times \exp\Big(-\gamma_{st} \int_0^{2\pi} \int_0^{d_{ti,t}^{\max}} \frac{\tau_s}{\tau_s + \frac{4\pi d_{ti,t}^2 (d_{t,b}^2 + d_{ti,t}^2 - 2d_{t,b} d_{ti,t} \cos(\psi))}{\rho_{st,i} d_{t,b}^2}} \times d_{ti,t} \mathrm{d}d_{ti,t} \mathrm{d}\psi\Big) \times 2\pi\gamma_{bs} d_{t,b} \exp(-\pi\gamma_{bs} d_{t,b}^2)\Big) \mathrm{d}d_{t,b}$$
$$\times \int_0^{r_{b,t}^{\max}} \Big(\exp\big(-(2^{\frac{r'_{c,com}}{B_c}} - 1) N_0 B_c f_c^2 r_{b,t}^{1.9} P_{c,t}^{-1} g_{c,b}^{-1} \times 10^{(0.1L_s - 2.8)}\big) \int_0^{r_{bj,tj}^{\max}} \exp\big(-2\pi\gamma_{bs} \frac{\arctan(\frac{C_d}{2r_{bj,tj}})}{\pi} \times \int_{r_{b,t}}^{r_{bj,t}^{\max}} \frac{(2^{\frac{r'_{c,com}}{B_c}} - 1) r_{bj,t}}{2^{\frac{r'_{c,com}}{B_c}} - 1 + (\frac{r_{bj,t}}{r_{b,t}})^{1.9}} \mathrm{d}r_{bj,t}\big) f_{R_{bj,tj}}(r_{bj,tj}) \times \mathrm{d}r_{bj,tj} 2\pi\gamma_{bs} r_{b,t} \exp(-\pi\gamma_{bs} r_{b,t}^2)\Big) \mathrm{d}r_{b,t} \quad (37)$$

where $d'_{t,b} = \min\big(d_{t,b}^{\max}, \frac{c}{2}(T_c - \frac{cT_c}{2B_s d'_{s,res}})\big)$.

Proof. See Appendix A. □

With the final expression of the joint CP in JSAC, we will verify the correctness of the analysis and obtain some system-level insights from the analysis results in the following section.

V. Numerical and Simulation Results

In this section, we provide the numerical results for the expressions derived throughout the paper. Before the presentation of the results, the parameters used in the calculation are shown in Table II, and some other parameters are presented later for different situations. All the Matlab related to this paper can be found on GitHub [40].

TABLE II: Table of Notations and Abbreviations.

Notation	Value
P_t, B , C_d	21 dBm [41], 4 GHz [41], 10 m
$g_{s,t}, g_{s,r}$, $\rho_{st}, \rho_{st,i}$	10 dB, 10 dB [41], 0.5, 0.5
T_c, N, F_n	40 ms, 100 [41], 13 dB [41]
$L_{gas} + L_{rain}$	0.7 dB/km [33], [34]
L_{add}, L_{imp}	20 dB, 5dB [36]
N_0, g_{cb}	-164 dB/Hz [36], 29.2 dB [42]

In Fig. 8, We plot the comparisons of the derived expression in Theorem 3 and the Monte-Carlo simulation. Regarding Fig. 8(a) and we have the parameters: γ_{st}=γ_{sct}=300 points/km^2, τ_s=0.01, $d'_{s,res}$=0.2 m, $r'_{c,com}$=0.5 Gbps, μ=η=0.5. Regarding Fig. 8(b), we have the parameters: $d'_{s,res}$=0.2 m, $\mu = \eta$=0.5, γ_{bs}=50 points/km^2, γ_{st}=γ_{sct}=300 points/km^2.

Firstly, we can see that the analysis results match the simulation results well, which confirms the validity of the analysis. With the given parameters shown in Fig. 8(a), applying the requirement of data rate instead of threshold in communication, we can see that the CPs increase with the increase of the BS density. However, when the BS density increases to a certain extent, improvement of the CPs is no longer noticeable, which indicates the existence of an optimal value for the density of BSs that maximizes coverage beyond which there is no point in further increasing the density. The stabilization of the communication coverage is consistent with Remark 2. In Fig. 8(b), there are two x-axises. The top x-axis indicates different values for the threshold in communication, and the bottom x-axis indicates different values for the threshold in

sensing. We can observe that the two separate CPs in S&C and the joint CP decrease with the increase of the two thresholds in S&C almost linearly, which is expected. Furthermore, since we know the joint coverage probability (CP) is the product of communication CP and sensing CP, as can be observed from Fig. 8(b), we can get the insight that we should keep communication and sensing CPs at a similar level to avoid the cripple on the joint CP. It means we should take care of the tradeoff for the resource allocation between sensing and communication. In the following, we will show the tradeoff between them and give insights about how to achieve the best performance with limited resources. In the following figures, to show the effects of the HDR in communication, the threshold in communication will be replaced as the requirement of HDR as discussed in (36).

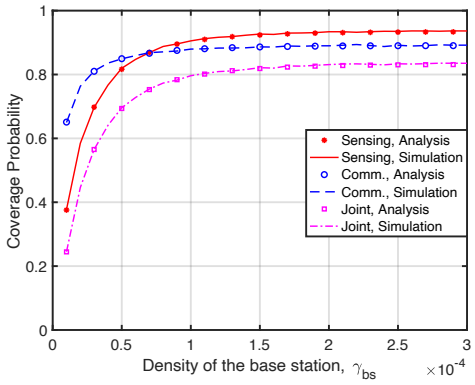

(a) The joint CP various with density of BS.

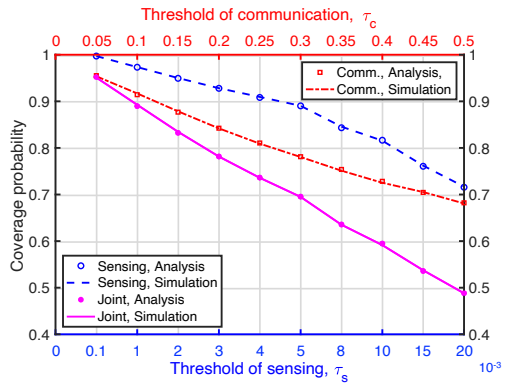

(b) The joint CP various with two thresholds in S&C.

Fig. 8: Comparison of the analysis and the simulation results.

The ergodic optimizations over the allocations of P&S for JSAC are shown in Fig. 9 with other parameters specified in the respective subfigure captions. First, we can observe that in a particular scenario, we can obtain the best allocations of P&S and achieve the best CP (the red star in the figures). Comparing Fig. 9(a) and Fig. 9(c) or Fig. 9(b) and Fig. 9(d), we can see that the maximum CP always happened at the lower bound of bandwidth in sensing which is related to the distance resolution, and it indicates that if we can tolerate a higher resolution, a higher CP might be achieved. Hence, we can have the insight that we should not pursue the redundancy of resolution too much in practical applications of JSAC (Generally speaking, when we design application system parameters, we will retain a certain amount of performance redundancy), since the preservation of the redundancy in sensing will cripple the joint performance of JSAC. Furthermore, comparing Fig. 9(a) and Fig. 9(b) or Fig. 9(c) and Fig. 9(d), we observe that the improvement of the optimized maximum CP is different. The improvement of the maximum CP (the red stars) from Fig. 9(a) to Fig. 9(b) is 0.84-0.73=0.11, and the improvement of the maximum CP from Fig. 9(c) to Fig. 9(d) is 0.87-0.78=0.09. For that setup, we can have the insight that if we want to improve the maximum CP via increasing the SDR in sensing or decreasing the HDR in communication, the latter option might be a better choice.

In Fig. 10, we plot the maximum CPs optimized over P&S with different densities of targets (including ST and SCT) and BSs. The four red stars in the four sub-figures are the four maximum CPs in each figure, which indicates the biggest CP that can be achieved with the related densities of the targets and the BSs, for the set of parameters given in the respective subfigure captions. Blue circles in the sub-figures are the maximum CP of each row, which denotes that with a given density of the targets, the best density of the BS can be calculated to achieve the best CP. Observing the Blue circles, we can find that with the increase of the target's density, the optimal BS density decreases. Insight can be given that if there is some information about the target density in practical application, the related optimal BS density can be set. If there is no information on the target density in practical application, the density of BS can be set as 150 to 200 points/km^2. Observing the developments of the maximum CP from Fig. 10(a) to Fig. 10(b) and from Fig. 10(c) to Fig. 10(d), the improvements are 0.90-0.82=0.08 and 0.92-0.86=0.06. Hence, the same insight can be obtained as indicated in Fig. 9. When we try to lose distance resolution or data rate to achieve a higher CP, the requirement of HDR can be released first.

Based on the ergodic optimizations over P&S and densities of targets and BSs, the CP performance of JSAC with different requirements of SDR and HSR are shown in Fig. 11(a). The range of SDR is [0.05,0.3] meters, and the range of HDR is [0.1,1] Gbps. As we can see, when the SDR is at a high level (a big SDR), the improvement of SDR will not decrease the joint CP critically. However, the improvement of HDR affects the joint CP almost linearly. Hence, we can obtain the insight that, constrained by the resources of P&S, if we want to release the requirements of SDR or HDR to improve the joint CP, with different situations, different choices should be made. For instance, when HDR is 1 Gbps and SDR is 0.05, releasing SDR to 0.1 will make a critical improvement on the joint CP. When the HDR=1 Gbps and SDR is 0.1 or higher, releasing HDR instead of SDR is a better option. Similarly, we also give the relationship between coverage probability and SDR under different HDRs in Fig. 11(b). We can clearly see that when HDR is at a high level and SDR at a small level, for example, HDR=1 Gbps, SDR=0.05 m, one step increase of SDR will make a significant step improvement on the CP. On the other hand, when the SDR is at a relatively high level, for example, SDR=0.2 m, an increase in SDR will not make a critical improvement on the CP, which means, in this case,

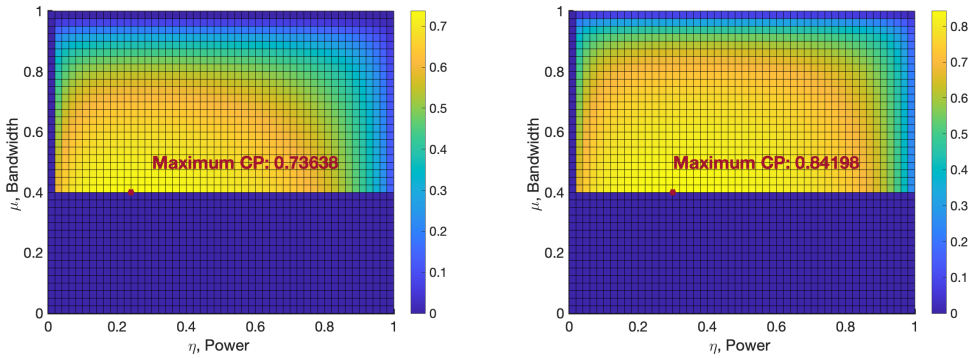

(a) CP, γ_{bs}=50 points/km^2, γ_{st}=γ_{sct}=500 points/km^2, $d'_{s,res}$=0.1 m, τ_s=0.001, $r'_{c,com}$=1 Gbps.

(b) CP, γ_{bs}=50 points/km^2, γ_{st}=γ_{sct}=500 points/km^2, $d'_{s,res}$=0.1 m, τ_s=0.001, $r'_{c,com}$=0.5 Gbps.

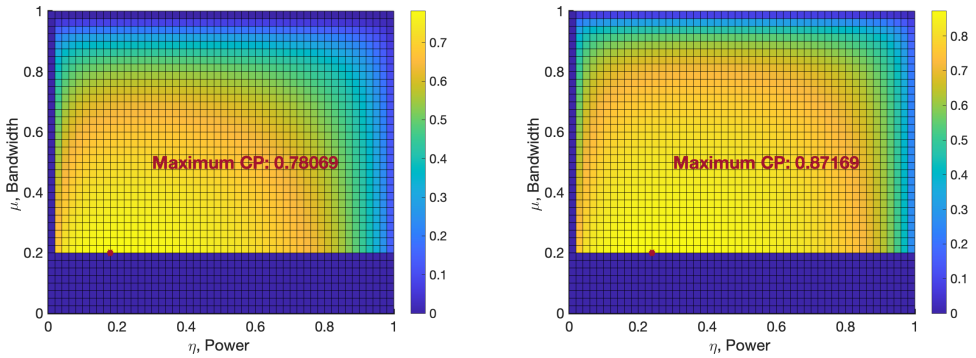

(c) CP, γ_{bs}=50 points/km^2, γ_{st}=γ_{sct}=500 points/km^2, $d'_{s,res}$=0.2 m, τ_s=0.001, $r'_{c,com}$=1 Gbps.

(d) CP, γ_{bs}=50 points/km^2, γ_{st}=γ_{sct}=500 points/km^2, $d'_{s,res}$=0.2 m, τ_s=0.001, $r'_{c,com}$=0.5 Gbps.

Fig. 9: CPs with different constraints of SDR and HDR.

we should use limited resources to prioritize improving HDR to obtain better improvement on CP.

VI. Conclusion and Future Work

In this paper, we have provided the first stochastic geometry-based performance evaluation considering the trade-off of the P&S between S&C in JSAC and achieved the ergodic optimizations. We focused on a practical application scenario of JSAC, where the densities of STs/SCTs and BS are involved. The drawn system-level insights from the analytical result in this paper can be beneficial for designing a practical application of JSAC. For instance, we provided a helpful guideline on the relationships between ST/SCT and BS densities. In addition, we provided insights on the performance limitations of the optimized CP, which can be a reference when the resources of JSAC are limited. This work can be extended in different directions. The design of the shared waveform between S&C can be studied to allocate the limited spectrum resources. The collaboration strategy of S&C can be studied in order to explore the extra benefit that S&C can obtain.

Appendix

A. The joint CP of JSAC

Considering the constraints of SDR and HDR revealed in Sec. IV-C, and taking $D_{t,b} \leq \frac{c}{2}\big(T_c - \frac{cT_c}{2B_s d'_{s,res}}\big)$ and $\tau_c = 2^{\frac{r'_{c,com}}{B_c}} - 1$ into the calculation of the joint CP, we can have

$$\begin{aligned}
\mathbb{P}_{\mathrm{j,cov}} &= \mathbb{P}\Big[\mathtt{SCNR}_s \geq \tau_s, D_{t,b} \leq \frac{c}{2}\big(T_c - \frac{cT_c}{2B_s d'_{s,res}}\big), \mathtt{SINR}_c \geq \tau_c\Big] \\
&= \underbrace{\mathbb{P}\big[\mathtt{SCNR}_s \times \mathbb{1}\big(D_{t,b} \leq \frac{c}{2}(T_c - \frac{cT_c}{2B_s d'_{s,res}})\big) \geq \tau_s\big]}_{(i)} \\
&\times \mathbb{P}\big[\mathtt{SINR}_c \geq 2^{\frac{r'_{c,com}}{B_c}} - 1\big] \qquad (38) \\
&\overset{(j)}{=} \int_0^{d'_{t,b}} \Bigg(\exp\big(-\tau_s K T_0 B_s F_n (P_{s,t} g_{s,t} g_{s,r} \rho_{st} c^2 N T_c)^{-1} \\
&\times (4\pi)^3 f_s^2 d_{t,b}^4 \big) \exp\big(-2\pi\gamma_{bs} \int_{d_{b,t}}^{d_{bj,t}^{\max}} \big(\frac{\tau_s}{\tau_s + (\frac{d_{bj,t}}{d_{t,b}})^2}\big) d_{bj,t} \mathrm{d}d_{bj,t} \big) \\
&\times \exp\Big(-\gamma_{st} \int_0^{2\pi} \int_0^{d_{ti,t}^{\max}} \frac{\tau_s}{\tau_s + \frac{4\pi d_{ti,t}^2 (d_{t,b}^2 + d_{ti,t}^2 - 2 d_{t,b} d_{ti,t} \cos(\psi))}{\rho_{st,i} d_{t,b}^2}} \\
&\times d_{ti,t} \mathrm{d}d_{ti,t} \mathrm{d}\psi \Big) \times 2\pi\gamma_{bs} d_{t,b} \exp(-\pi\gamma_{bs} d_{t,b}^2) \Bigg) \mathrm{d}d_{t,b} \\
&\times \int_0^{r_{b,t}^{\max}} \Bigg(\exp\big(-(2^{\frac{r'_{c,com}}{B_c}} - 1) N_0 B_c f_c^2 r_{b,t}^{1.9} P_{c,t}^{-1} g_{c,b}^{-1} \\
&\times 10^{(0.1 L_s - 2.8)} \big) \int_0^{r_{bj,tj}^{\max}} \exp\Big(-2\pi\gamma_{bs} \frac{\arctan(\frac{C_d}{2r_{bj,tj}})}{\pi}
\end{aligned}$$

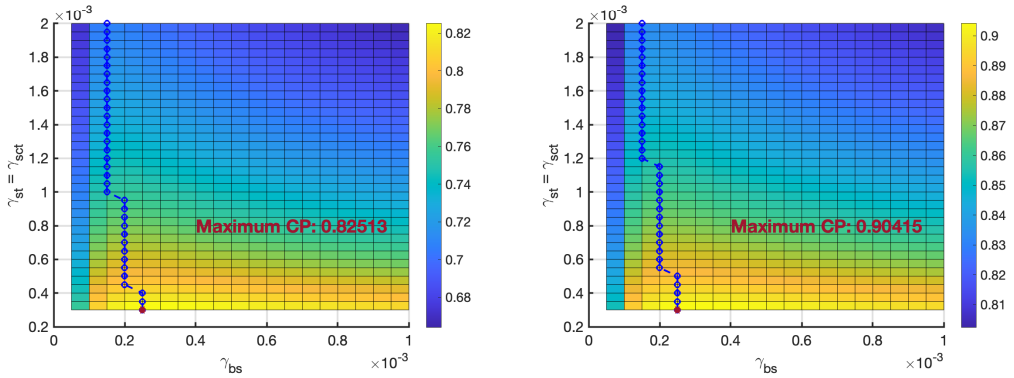

(a) CP, $d'_{s,res}$=0.1 m, τ_s=0.001, $r'_{c,com}$=1 Gbps.

(b) CP, $d'_{s,res}$=0.1 m, τ_s=0.001, $r'_{c,com}$=0.5 Gbps.

(c) CP, $d'_{s,res}$=0.2 m, τ_s=0.001, $r'_{c,com}$=1 Gbps.

(d) CP, $d'_{s,res}$=0.2 m, τ_s=0.001, $r'_{c,com}$=0.5 Gbps.

Fig. 10: CPs with different constraints of SDR and HDR.

$$\times \int_{r_{b,t}}^{r_{bj,t}^{\max}} \frac{(2^{\frac{r'_{c,com}}{B_c}}-1)r_{bj,t}}{2^{\frac{r'_{c,com}}{B_c}}-1+(\frac{r_{bj,t}}{r_{b,t}})^{1.9}} \mathrm{d}r_{bj,t}) f_{R_{bj,tj}}(r_{bj,tj}) \mathrm{d}r_{bj,tj}$$

$$\times 2\pi\gamma_{bs} r_{b,t} \exp(-\pi\gamma_{bs} r_{b,t}^2)\Big) \mathrm{d}r_{b,t} \quad (39)$$

where $\mathbb{1}(x<y)$ means indicator function (if the input, $x<y$, is true, the output is 1, else, the output is 0), the step (j) regarding the part (i) in (38) is calculated from the fact that $\mathtt{SCNR}_s$ is an integral function based on the range of $D_{t,b}$ as shown in Theorem 1, hence, the upper bounds of $D_{t,b}$ caused by the SDR can be transformed as the upper bound of the integration shown in (28), $d'_{t,b} = \min\left(d_{t,b}^{\max}, \frac{c}{2}(T_c - \frac{cT_c}{2B_s d'_{s,res}})\right)$.

REFERENCES

[1] N. Kouzayha, H. Elsawy, H. Dahrouj, K. Alshaikh, T. Y. Al-Naffouri, and M.-S. Alouini, "Analysis of large scale aerial terrestrial networks with mmWave backhauling," *IEEE Transactions on Wireless Communications*, vol. 20, no. 12, pp. 8362–8380, 2021.

[2] A. Faisal, H. Sarieddeen, H. Dahrouj, T. Y. Al-Naffouri, and M.-S. Alouini, "Ultramassive MIMO systems at terahertz bands: Prospects and challenges," *IEEE Vehicular Technology Magazine*, vol. 15, no. 4, pp. 33–42, 2020.

[3] H. Chen, H. Sarieddeen, T. Ballal, H. Wymeersch, M.-S. Alouini, and T. Y. Al-Naffouri, "A tutorial on terahertz-band localization for 6G communication systems," *IEEE Communications Surveys & Tutorials*, vol. 24, no. 3, pp. 1780–1815, 2022.

[4] H. Sarieddeen, N. Saeed, T. Y. Al-Naffouri, and M.-S. Alouini, "Next generation terahertz communications: A rendezvous of sensing, imaging, and localization," *IEEE Communications Magazine*, vol. 58, no. 5, pp. 69–75, 2020.

[5] X. Fang, W. Feng, Y. Chen, N. Ge, and Y. Zhang, "Joint communication and sensing toward 6G: Models and potential of using MIMO," *IEEE Internet of Things Journal*, vol. 10, no. 5, pp. 4093–4116, 2023.

[6] J. A. Zhang *et al.*, "Enabling joint communication and radar sensing in mobile networks—a survey," *IEEE Communications Surveys & Tutorials*, vol. 24, no. 1, pp. 306–345, 2022.

[7] F. Liu, Y. Cui, C. Masouros, J. Xu, T. X. Han, Y. C. Eldar, and S. Buzzi, "Integrated sensing and communications: Toward dual-functional wireless networks for 6G and beyond," *IEEE Journal on Selected Areas in Communications*, vol. 40, no. 6, pp. 1728–1767, 2022.

[8] Ericsson, "Joint communication and sensing in 6G networks," Available at https://www.ericsson.com/en/blog/2021/10/joint-sensing-and-communication-6g, accessed Mar. 25, 2023.

[9] Huawei, "Integrated sensing and communication (ISAC) — from concept to practice," Available at https://www.huawei.com/en/huaweitech/future-technologies, accessed Mar. 22, 2023.

[10] X. You *et al.*, "Towards 6G wireless communication networks: vision, enabling technologies, and new paradigm shifts," *Science China Information Sciences*, vol. 64, no. 1, p. 110301, Jan 2021.

[11] Y. Chen, J. Zhang, W. Feng, and M.-S. Alouini, "Radio sensing using 5G signals: Concepts, state of the art, and challenges," *IEEE Internet of Things Journal*, vol. 9, no. 2, pp. 1037–1052, 2022.

[12] O. Li *et al.*, "Integrated sensing and communication in 6G: a prototype of high resolution multichannel THz sensing on portable device," *EURASIP Journal on Wireless Communications and Networking*, vol. 2022, no. 1, p. 106, Oct 2022.

[13] J. Wang, N. Varshney, C. Gentile, S. Blandino, J. Chuang, and N. Golmie, "Integrated sensing and communication: Enabling techniques, applications, tools and data sets, standardization, and future directions," *IEEE Internet of Things Journal*, vol. 9, no. 23, pp. 23 416–23 440, 2022.

[14] U. Demirhan and A. Alkhateeb, "Integrated sensing and communication for 6G: Ten key machine learning roles," Dec 2022, arXiv:2208.02157. [Online]. Available: http://arxiv.org/abs/2208.02157

[15] K. Meng, Q. Wu, S. Ma, W. Chen, K. Wang, and J. Li, "Throughput

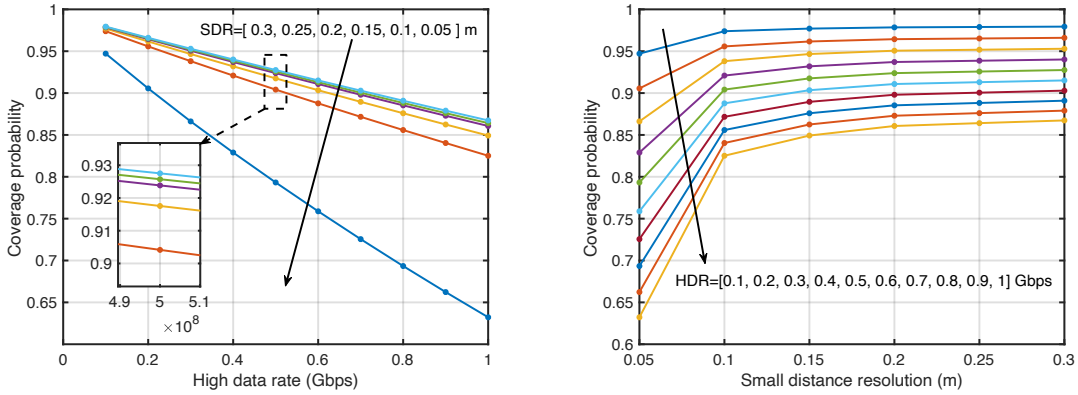

(a) (b)

Fig. 11: Coverage probability varies with HDR and SDR.

maximization for UAV-enabled integrated periodic sensing and communication," *IEEE Transactions on Wireless Communications*, vol. 22, no. 1, p. 671–687, Jan 2023.

[16] F. Dong, W. Wang, X. Li, F. Liu, S. Chen, and L. Hanzo, "Joint beamforming design for dual-functional MIMO radar and communication systems guaranteeing physical layer security," *IEEE Transactions on Green Communications and Networking*, vol. 7, no. 1, pp. 537–549, 2023.

[17] D. Cong, S. Guo, H. Zhang, J. Ye, and M.-S. Alouini, "Beamforming design for integrated sensing and communication systems with finite alphabet input," *IEEE Wireless Communications Letters*, vol. 11, no. 10, pp. 2190–2194, 2022.

[18] Z. Fang, Z. Wei, X. Chen, H. Wu, and Z. Feng, "Stochastic geometry for automotive radar interference with rcs characteristics," *IEEE Wireless Communications Letters*, vol. 9, no. 11, pp. 1817–1820, 2020.

[19] N. R. Olson, J. G. Andrews, and R. W. Heath Jr, "Coverage and capacity of joint communication and sensing in wireless networks," Oct 2022, arXiv:2210.02289. [Online]. Available: http://arxiv.org/abs/2210.02289

[20] K. S. Ali and M. Chafii, "Integrated sensing and communication for large networks using a dynamic transmission strategy and full duplex," Nov 2022, arXiv:2211.09466. [Online]. Available: http://arxiv.org/abs/2211.09466

[21] D. Ghozlani, A. Omri, S. Bouallegue, H. Chamkhia, and R. Bouallegue, "Stochastic geometry-based analysis of joint radar and communication-enabled cooperative detection systems," in *2021 17th International Conference on Wireless and Mobile Computing, Networking and Communications (WiMob)*, Oct 2021, p. 325–330.

[22] F. D. S. Moulin, C. Wiame, L. Vandendorpe, and C. Oestges, "Joint performance metrics for integrated sensing and communication systems in automotive scenarios," Aug 2022, arXiv:2208.12790. [Online]. Available: http://arxiv.org/abs/2208.12790

[23] Z. Fang, Z. Wei, Z. Feng, X. Chen, and Z. Guo, "Performance of joint radar and communication enabled cooperative detection," in *2019 IEEE/CIC International Conference on Communications in China (ICCC)*, Aug 2019, p. 753–758.

[24] Y. Nabil, H. ElSawy, S. Al–Dharrab, H. Attia, and H. Mostafa, "A stochastic geometry analysis for joint radar communication system in millimeter-wave band," in *ICC 2023 - IEEE International Conference on Communications*, 2023, pp. 5849–5854.

[25] P. Ren, A. Munari, and M. Petrova, "Performance tradeoffs of joint radar-communication networks," *IEEE Wireless Communications Letters*, vol. 8, no. 1, pp. 165–168, 2019.

[26] S. S. Ram and G. Ghatak, "Optimization of network throughput of joint radar communication system using stochastic geometry," Jan 2022, arXiv:2201.03221. [Online]. Available: http://arxiv.org/abs/2201.03221

[27] B. K. Chalise, M. G. Amin, and B. Himed, "Performance tradeoff in a unified passive radar and communications system," *IEEE Signal Processing Letters*, vol. 24, no. 9, p. 1275–1279, Sep 2017.

[28] B. K. Chalise and B. Himed, "Performance tradeoff in a unified multistatic passive radar and communication system," in *2018 IEEE Radar Conference (RadarConf18)*, Apr 2018, p. 0653–0658.

[29] M. I. Skolnik, *Radar handbook*. McGraw-Hill Education, 2008.

[30] "P.1411-10: Propagation data and prediction methods for the planning of short-range outdoor radiocommunication systems and radio local area networks in the frequency range 300 MHz to 100 GHz," available at https://www.itu.int/rec/R-REC-P.1411/en, accessed Nov. 20, 2021.

[31] "P.676-13: Attenuation by atmospheric gases and related effects," available at https://www.itu.int/rec/R-REC-P.676, accessed Nov. 20, 2021.

[32] "P.530-18: Propagation data and prediction methods required for the design of terrestrial line-of-sight systems," available at https://www.itu.int/rec/R-REC-P.530-18-202109-I/en, accessed Nov. 20, 2021.

[33] L. Ippolito, "Radio propagation for space communications systems," *Proceedings of the IEEE*, vol. 69, no. 6, p. 697–727, Jun 1981.

[34] Y. Niu, Y. Li, D. Jin, L. Su, and A. V. Vasilakos, "A survey of millimeter wave (mmwave) communications for 5G: Opportunities and challenges," Feb 2015, arXiv:1502.07228. [Online]. Available: http://arxiv.org/abs/1502.07228

[35] T. S. Rappaport, S. Sun, R. Mayzus, H. Zhao, Y. Azar, K. Wang, G. N. Wong, J. K. Schulz, M. Samimi, and F. Gutierrez, "Millimeter wave mobile communications for 5G cellular: It will work!" *IEEE Access*, vol. 1, p. 335–349, 2013.

[36] S. Kutty and D. Sen, "Beamforming for millimeter wave communications: An inclusive survey," *IEEE Communications Surveys & Tutorials*, vol. 18, no. 2, p. 949–973, 2016.

[37] "IEEE standard for radar definitions," *IEEE Std 686-2017 (Revision of IEEE Std 686-2008)*, Sept. 2017.

[38] J. G. Andrews, A. K. Gupta, and H. S. Dhillon, "A primer on cellular network analysis using stochastic geometry," Oct 2016, arXiv: 1604.03183. [Online]. Available: http://arxiv.org/abs/1604.03183

[39] J. Xu, M. A. Kishk, and M.-S. Alouini, "Coverage enhancement of underwater internet of things using multilevel acoustic communication networks," *IEEE Internet of Things Journal*, vol. 9, no. 24, pp. 25 373–25 385, 2022.

[40] J. Xu, "Matlab-for-papers_jiajie-xu," Available at https://github.com/xujiajie112358/Matlab-for-papers_jiajie-xu, accessed Dec. 18, 2023.

[41] "AWR2944 single-chip 76- and 81-Ghz FMCW radar sensor datasheet." Available at https://www.ti.com/product/AWR2944, accessed Mar. 20, 2023.

[42] X. Wang *et al.*, "Millimeter wave communication: A comprehensive survey," *IEEE Communications Surveys & Tutorials*, vol. 20, no. 3, pp. 1616–1653, 2018.

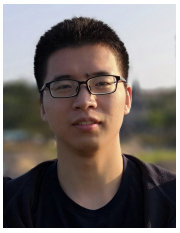

Jiajie Xu [S'19, M'24] received his M.Sc. and Ph.D. degrees from Yanshan University and King Abdullah University of Science and Technology (KAUST) in 2019 and 2023. He is a postdoctoral research fellow in the communication theory lab at KAUST. His current research interests include underwater wireless acoustic communication, underwater target detection, underwater cooperative networks, maritime communication, space-air-ground-sea integrated communication systems and joint sensing and communication systems, stochastic geometry, and energy harvesting wireless networks.

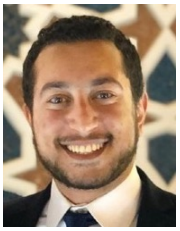

Mustafa A. Kishk [S'16, M'18] received the B.Sc. and M.Sc. degrees from Cairo University, Giza, Egypt, in 2013 and 2015, respectively, and the Ph.D. degree from Virginia Tech, Blacksburg, VA, USA, in 2018, all in Electrical Engineering. He is an assistant professor at the Electronic Engineering Department, Maynooth University, Ireland. Before that, he was a Postdoctoral Research Fellow with the Communication Theory Laboratory at King Abdullah University of Science and Technology, Saudi Arabia. He currently serves as an associate editor with IEEE Wireless Communication Letters. His current research interests include stochastic geometry, UAV-enabled communication systems, and satellite-enabled communications. He is a recipient of the IEEE ComSoc Outstanding Young Researcher Award for Europe, the Middle East, and Africa Region in 2022. He was recognized as an Exemplary Reviewer by the IEEE Communications Letters in 2020.

Justin P. Coon (Senior Member, IEEE) received the B.Sc. degree (with distinction) in electrical engineering from Calhoun Honours College, Clemson University, Clemson, SC, USA, in 2000 and the Ph.D. degree in communications from the University of Bristol, Bristol, U.K., in 2005. He held various research positions with Toshiba Research Europe Ltd. (TREL) from 2004 to 2013, including the position of a Research Manager from 2010 to 2013, during which, he led all research on physical layer communications and network science with TREL. In 2013, he joined the University of Oxford, Oxford, U.K. He has authored or coauthored more than 200 papers in IEEE and APS journals and conferences and is a named Inventor on more than 30 patents. He was the recipient of the Toshiba's Distinguished Research Award for his work on 4G systems and three best paper awards. He was the Editor of several IEEE journals and has Chaired or Co-chaired various conferences. He is a Fellow of the Institute for Mathematics and its Applications.

Mohamed-Slim Alouini [S'94-M'98-SM'03-F'09] was born in Tunis, Tunisia. He received the Ph.D. degree in Electrical Engineering from the California Institute of Technology (Caltech) in 1998. He served as a faculty member at the University of Minnesota then in the Texas A&M University at Qatar before joining in 2009 the King Abdullah University of Science and Technology (KAUST) where he is now a Distinguished Professor of Electrical and Computer Engineering. Prof. Alouini is a Fellow of the IEEE and of the OSA. He is currently particularly interested in addressing the technical challenges associated with the uneven distribution, access to, and use of information and communication technologies in far-flung, rural, low-density populations, low-income, and/or hard-to-reach areas.